

**International Meeting on Data for Atomic and Molecular
Processes in Plasmas: Advances in Standards and Modelling**

November 12-15, 2024, Palić, Serbia

**BOOK OF ABSTRACTS AND
CONTRIBUTED PAPERS**

Edited by Vladimir A. Srećković, Aleksandra Kolarski,
Milica Langović, Filip Arnaut and Nikola Veselinović

Belgrade, 2024

Scientific Organizing Committee

Vladimir A. Srećković, Institute of Physics Belgrade, **Co-Chair**
Aleksandra Kolarski, Institute of Physics Belgrade, **Co-Chair**

Milan S. Dimitrijević, Serbia
Nikolai N. Bezuglov, Russia
Nebil Ben Nessib, Saudi Arabia
Vesna Borka Jovanović, Serbia
Nikola Cvetanović, Serbia
Saša Dujko, Serbia
Rafik Hamdi, Tunisia
Magdalena Hristova, Bulgaria
Ognyan Kounchev, Bulgaria
Bratislav Marinković, Serbia
Zoran Mijić, Serbia
Nicolina Pop, Romania
Luka Popović, Serbia
Branko Predojević, Republic of Srpska, BiH
Sylvie Sahal Brechot, France
Sanja Tošić, Serbia
Robert Beuc, Croatia
Felix Iacob, Romania

Local Organizing Committee

Aleksandra Kolarski (**Co-Chair**), Institute of Physics Belgrade
Vladimir A. Srećković (**Co-Chair**), Institute of Physics Belgrade
Filip Arnaut (**Secretary**), Institute of Physics Belgrade
Zoran Mijić, Institute of Physics Belgrade
Milica Langović, Institute of Physics Belgrade
Mihailo Savić, Institute of Physics Belgrade
Nikola Veselinović, Institute of Physics Belgrade
Veljko Vujčić, Astronomical Observatory, Belgrade
Nikola Cvetanović, University of Belgrade, Faculty of Transport and Traffic Eng.

Organizer

Institute of Physics Belgrade

ISBN 978-86-82441-69-4

Published and copyright by: Institute of Physics Belgrade

Printed by: Skripta Internacional, Mike Alasa 54, 11102, Beograd

Number of copies: 50

SCIENTIFIC RATIONALE

Efficiency of theoretical analysis, synthesis and modeling of various environments, depends on atomic data and their sources. In particular, for the modeling of stellar atmospheres and opacity calculations a large number of atomic data is needed, since we do not know a priori the chemical composition of a stellar atmosphere. The same holds for Earth observations. Consequently, the development of databases with atomic data as well as astro-geoinformatics is important. This meeting will bring together physicists, astro & geophysicists from Serbia and elsewhere to review the present stage of research in this field. The meeting is planned as an opportunity to consider the above-mentioned aspects of spectroscopic research on plenary sessions and then to work on the special mini-projects, which will result in common papers to be published in international scientific journals.

Venue

Palić, (Hotel Prezident – Palić), Serbia

CONTENTS

Plenary Invited Lectures

- Dimitrijević, M.S.
Spectral line broadening and the corresponding databases 10

Invited Lectures

- Kolarski, A.
Earth's Lower Ionosphere impacted by High Class X-Ray Solar Flare Events 12

- Iacob, F.
Pseudo harmonic oscillator potential 22

- Pop, N., Djuissi, E., Mezei, J.Z. and Schneider, I.F.
Reactive collisions between electrons and molecular cations. Applications in astrophysics and cold plasmas modelling 23

- Milosavljevic, A.R., Nicolas, C., Robert, E. and Bozek, J.
Soft x-ray photoelectron-photoion-photoion coincidence (PEPIPICO) spectroscopy of isolated molecular systems at PLEIADES beamline (SOLEIL synchrotron) 25

- Kounchev, O. and Simeonov, G.
Neural Networks in Astrophysics and Plasma Physics: Transformers, PINNs, KANNs, and all that 26

- Dujko, S., Simonović, I.B. and Bošnjaković, D.V.
Kinetic and fluid studies on Resistive Plate Chambers operated with new eco-friendly gas mixtures 27

Lectures

- Borka Jovanović, V., Borka, D. and Jovanović, P.
X-shaped radio galaxy 3C 315 30

- Starčević, N. and Petrović, S.
Study of very thin crystals by rainbow scattering effect 40

- Savić, M.R., Veselinović, N.B., Dragić, A.L., Maletić, D.M., Joković, D.R., Banjanac, R.M., Knežević, D., Travar, M. and Udovičić, V.I.
Implications of the Temperature Effect Analysis Using Simulated Secondary Cosmic Muon Data 47

Mijić, Z.R. and Marinković, B.P. <i>New opportunities for COST participants – actions networking tools and examples of the national funding schemes</i>	49
<i>Posters</i>	
Eichelberger, H., Nina, A., Boudjada, M.Y., Kolarski, A., Veselinović, N.B., Nico, G., Biagi, P.F. and Srećković, V.A. <i>Terminator variations of VLF/LF amplitudes - observational techniques and case studies</i>	52
Nina, A., Butka, P., Kolarski, A., Srećković, V.A., Sarnovský, M., Bednár, P. and Popović, L.Č. <i>Specific changes in VLF signals induced by astrophysical and geophysical phenomena: possibility of applying machine learning in statistical analyses</i>	59
Srećković, V.A., Iacob, F. and Vujčić, V. <i>Investigating Collisional and Radiative Processes: Important Datasets for Molecular Dynamics</i>	65
Srećković, V.A., Pop, N., Vujčić, V., Dimitrijević, M.S., Christova, M.D. and Mijić, Z. <i>New molecular dataset for planet formation chemistry and modeling</i>	67
Kolarski, A., Nina, A., Srećković, V.A., Arnaut, F. and Langović, M. <i>Earth's Lower Ionosphere under energetic events: solar flares and gamma ray bursts as drivers for VLF signal perturbations</i>	69
Tošić, S., Srećković, V.A. and Vujčić, V. <i>Photodissociation processes in non-symmetric systems</i>	70
Arnaud, F., Kolarski, A., Langović, M., Srećković, V.A. and Jevremović, S. <i>Machine Learning Classification Difficulties of VLF Amplitude Variations Around the Terminator</i>	71
Marjanović, J., Marić, D., Dujko, S. and Petrović, Z.Lj. <i>Electrical Breakdown in trans-1,3,3,3-Tetrafluoropropene HFO1234ze(E)</i>	72
Marinković, B.P., Ivanović, S.Đ. and Uskoković, N.A. <i>Elastic electron scattering by xenon atom and data coverage within BEAMDB</i>	74
Simonović, I.B., Bošnjaković, D.V. and Dujko, S. <i>Fitting of the current signal of the Pulsed Townsend experiment with the gradient descent algorithm</i>	75

Krstić, I.B., Obradović, B.M. and Kuraica, M.M. <i>Spatio-temporal dynamics of a microsecond pulsed glow discharge</i>	77
Sretenović, G.B., Kovačević, V.V., Obradović, B.M., Kuraica, M.M. and Ranitović, P. <i>Helium plasma jet as a probe for the laser irradiance measurements</i>	79
Maljković, J.B., Marinković, B.P. and Kopyra, J. <i>Dissociative electron attachment to isoflurane molecule in the gas phase</i>	81
Borka Jovanović, V., Borka, D., Capozziello, S. and Jovanović, P. <i>Constraining the Deser-Woodard non-local gravity by Fundamental plane of elliptical galaxies</i>	82
Petrović, V.M., Delibašić Marković, H.S. and Petrović, I.D. <i>Impact of Coulomb correction on the nonadiabatic tunnel ionization in an elliptically polarized laser field</i>	84
Jovanović, P., Borka Jovanović, V. and Borka, D. <i>Bounds on graviton mass from astrometric data of S-stars</i>	86
SECTIONS (MINI PROJECTS)	88
PROGRAMME	89
AUTHORS' INDEX	93

Plenary Invited Lectures

Spectral line broadening and the corresponding databases

Dimitrijević, M.S.^{1,2} 

¹*Astronomical Observatory, Volgina 7, 11060 Belgrade, Serbia*

²*LERMA, Observatoire de Paris, Université PSL, CNRS, Sorbonne Université,
5 Place Jules Janssen, 92190 Meudon, France*

E-mail: mdimitrijevic@ipb.ac.rs

Profiles of spectral lines broadened by collisions with charged particles (Stark broadening) and neutral atoms (Van der Waals and resonance broadening) are needed for determination of various quantities and solution of different problems in astrophysics, physics and technology, as for example modelling of stellar plasma, analysis and synthesis of spectral lines, calculations of absorption coefficient, opacity, radiative transfer, abundance determination, laboratory plasma diagnostic, lasers and laser produced plasma, inertial fusion experiments and modelling and optimisation of plasmas in technology.

In this contribution we will present databases containing data relevant to the broadening of atomic and ionic spectral lines, needed for above mentioned topics. We will discuss and describe Atomic Spectral Line Broadening Bibliographic Database of National Institute of Standards and Technology (NIST - Washington); the Vienna Atomic Line Database (VALD), a collection of atomic and molecular transition parameters of astronomical interest (Piskunov et al. 1995); the collection of databases of Paris Observatory: MOLAT Atomic and Molecular Data containing, among others, three databases of interest for line profiles: BALSS (Bibliography of Atomic Line Shapes and Shifts), Griem's tables (Griem 1974) and STARK-B database containing data on Stark broadening parameters (Sahal-Bréchet et al. 2015). Additionally we will present and VAMDC, european Virtual Atomic and Molecular Data Center. Also, we will discuss where the data on spectral line profiles may be used.

References

- Dubernet M., Boudon, L. V., Culhane, J. L., Dimitrijević, M. S., et al., 2010, *J. Quant. Spectrosc. Radiat. Transfer*, 111, 2151
Griem, H. R., 1974, *Spectral line broadening by plasmas*, Academic press
Piskunov et al., 1995, *Astron. Astrophys. Suppl.*, 112, 525
Sahal-Bréchet S., Dimitrijević M. S., Moreau N., Ben Nessib N., 2015, *Phys. Scr.*, 50, 054008

Invited Lectures

Earth's Lower Ionosphere impacted by High Class X-Ray Solar Flare Events

Kolarski, A.¹ 

¹ *Institute of Physics Belgrade, University of Belgrade, Pregrevica 118, 11000 Belgrade, Serbia*

E-mail: aleksandra.kolarski@ipb.ac.rs

Abstract

Solar activity, especially with its energetic events like solar flares and coronal mass ejections of high intensity, triggers abrupt and strong disturbances within near Earth surroundings, posing the potential hazard to numerous sophisticated technological systems both space-borne and ground-based on one hand, and putting at risk all living life on our planet on the other. Direct influences of events like geomagnetic storms and solar flares on human health were reported in literature. In this paper effects of high class X-ray solar flares from descending branch of 24th solar cycle were analyzed in terms of associated mid-latitude lower ionospheric disturbances over European sector, based on simultaneously monitored Very Low Frequency signals' perturbations as recorded by ground-based receiving system located in Belgrade, Serbia. Conducted numerical simulations revealed electron density increases of several orders of magnitude during maximal impact of analyzed solar flare events.

Key words: Solar activity, X-ray flares, ionosphere, VLF signal, perturbation

Introduction

Complex solar-terrestrial interactions between Sun and Earth have been in scientific focus for many decades, however only in recent past many governmental space agencies and observatories made their data, related to space weather, sun activity and satellite observations, both current and archived, publicly available, which combined with open access policies and in general broader information availability made space- and geo-sciences more approachable and more present in everyday life (see websites of major national space agencies, such as e.g. NOAA National Centers for Environmental Information, ESA Space Weather services, Center of Excellence in Space Sciences India, IISER Kolkata, Australian space weather forecasting center, Worldwide Archive of Low-Frequency Data and

Observations, Geostationary Operational Environmental Satellite (GOES) archive database, Royal Observatory of Belgium etc.).

Sun's continually emitted radiation, both of the electromagnetic and corpuscular nature, directly influence Earth's surroundings in terms of affecting and perturbing Earth's magnetosphere and ionosphere regions (e.g. Kelly 2009, Hayes et al. 2021, Rycroft et al. 2000 and references therein). Enhanced dependences on sophisticated technologies (like satellites, telecommunications, power grid systems) with globally increasing demands from modern societies made solar activity recognized and validated as potential hazard, to these systems and also to all living beings on our planet and space crews as well (e.g. Riley and Love 2017, Eastwood et al. 2017, Yasyukevich et al. 2018). An increasing overpopulation problems on Earth, in relation to more frequent and more intense severe weather conditions, as well with oft and at locations that are not so typical for their occurrences, along with general ongoing climate changes (e.g. Cramer et al. 2021, IPCC 2023, Martinich and Crimmins 2019), peaked interest of common people regarding possibly dangerous events of extraterrestrial origin (originating both from our solar system and beyond, like solar flares (SFs), coronal mass ejections (CMEs), gamma ray bursts (GRBs), etc.).

Complex solar activity, especially regarding energetic solar events, like intense SFs and CMEs and their interactions, is still unpredictable to solar physics, both regarding their occurrences and features. Such events, their interactions and impacts on near Earth environment are commonly presented as case studies, covering wide range of related phenomena and observational "points of view" (e.g. Manju et al. 2009, Sahai et al. 2007, Barta et al. 2022, Srećković et al. 2021, Kolarski et al. 2023).

Analysis and results

In this paper, active solar periods of the 24th solar cycle descending branch were investigated, with X-class X-ray solar flare events accompanied with CMEs given the special interest. Solar conditions during September 2017 and their geo-effective implications are presented as a case study, through observations conducted by employing Very Low Frequency (VLF) technology (e.g. Silber and Price 2017 and references therein). Ground-based Absolute Phase and Amplitude Logger (AbsPAL) system located in Belgrade (Serbia) at the Institute of physics (44.85°N; 20.38°E) operating in narrow-band mode was utilized for monitoring VLF signals' perturbations related to subionospheric propagation within Earth-ionosphere waveguide. Ionospheric parameters (Wait and Spies 1964) were retrieved by numerical modeling procedure (e.g. Silber and Price 2017 and references therein, Srećković et al. 2021, Kolarski et al. 2023, Thomson et al. 2005, McRar and Thomson 2004, Kolarski and Grubor 2014, Grubor et al. 2008, Šulić et al. 2016, Žigman et al. 2007, etc.) using Long Wave Propagation Capability (LWPC)

software (Ferguson 1998). Soft X-ray flux (0.1-0.8 nm) solar data were taken from Geostationary Operational Environmental Satellite (GOES) archive database.

During 2017, Sun showed unusual activity in relation to both occurrences of solar flares and their strengths and of producing coronal mass ejections, taking into consideration how “late” in the solar cycle this activity emerged, practically right before the solar minimum between 24th and 25th SCs (in December 2019). In general, the 24th SC had notably decreased activity compared to several previous cycles. This SC had also the fourth smallest intensity since the 1st SC. Within SC with such “quiet” activity, and especially taking into consideration that is placed practically next to the solar minimum between 24th and 25th SCs, year of 2017 is striking primarily for two reasons: strongest of the SFs within entire 24th SC occurred during only one month of this year – September 2017 and also due to the abundance of produced SFs during this month (Tables 1 and 2). Aside especially active period during September (with 99 SFs reported, including 27 M-class and 4 X-class events), month of April (with 52 SFs reported, with 7 M-class and without X-class events) also stands out.

The most active period in 2017 was by far month of September, when 4 X-class SFs were reported: X2.2 and X9.3 occurred on September 6th, X1.3 occurred on September 7th and X8.2 occurred on September 10th. Two strongest among them, i.e. X9.3 and X8.2 are being the strongest reported SFs of the entire 24th SC. During September, the strongest M-class SFs of the year 2017 were reported: M8.1 occurred on September 8th and M7.3 occurred on September 7th. X-class SFs from September 2017 are listed in Table 3 (an original data, with applied scalar). Most of the activity and all of the strongest SFs of September 2017 are related to the same active region AR2673, which had very complex and unusual evolution producing in total 77 SFs, including 1 of B-, 45 of C-, 27 of M- and 4 of X-class events. During September 6th, 7th and 10th, R3 radio blackouts related to X-class SFs of X2.2, X9.3, X1.3 and X8.2 respectively, were reported. Related to accompanying CMEs, geomagnetic storms up to G4 were reported, as well.

It is interesting to note that SF X9.3 hasn't been reported for two decades: event of similar strength dated back as far to November 6th, 1997 (X9.4) - interestingly also close to solar minimum, but on ascending branch of 23rd SC. One slightly weaker event occurred about one decade ago on December 5th, 2006 (X9) - interestingly also close to solar minimum and in descending branch of 23rd SC. Closest in time and of X-class, although significantly weaker in strength, was X2.7 reported on May 5th, 2015 - close to 24th SC solar maximum. Compared to X9.3 from September 2017, some weaker X-class SFs in period August-December were also reported over the years (e.g. in 2011 (X6.9), 2006 (X6.5), 2005 (X6.2) and 2005 (X5.4)) related to SCs' branches and some significantly stronger SFs (e.g. in 2005 (X17+), 2003 (X28+) and 2001 (X20+)), related to SCs' branches and activity maximum.

Earth's mid-litudinal lower ionosphere impacted by high class X-Ray SFs from September 2017 was explored by remote sensing approach, employing ground-based equipment system located in Belgrade and using simultaneous multi-VLF signal monitoring technique. In terms of applied technology, Earth's lower ionosphere firmly responded to and followed incident soft X-ray radiation, with time delay corresponding to sluggishness of the ionosphere (Žigman et al. 2007, Appleton 1953), revealing intense perturbations both in amplitude and phase delays of recorded VLF signals. Perturbations monitored on VLF GQD signal related to high class X-Ray SFs from September 2017 and recorded by AbsPAL narrow-band system located in Belgrade are analyzed and presented in this study. The GQD signal is emitted from Skelton UK (54.72°N; 2.88°W) on frequency 22.1 kHz and arrives to Belgrade (44.85°N; 20.38°E) from north in NW-SE direction, propagating mostly over land, with Great Circle Path (GCP) of 1982 km, covering almost two time zones.

Solar X-ray irradiances of soft range (0.1-0.8 nm) corresponding to the most active days during September 2017 related to X-class solar flares are given in Figure 1. GQD signal amplitude and phase perturbations induced by these high class X-Ray SFs and recorded in Belgrade are given in Figure 2. Perturbations of GQD signal recorded in Belgrade, induced by these high class X-ray SFs, reached up to 8 dB in amplitude and up to a few tens of degrees in phase, compared to unperturbed ionospheric conditions. Based on recorded amplitude and phase perturbations, modeling of propagation parameters based on utilization of LWPC software was conducted, with goal that output parameters corresponding to modeled and input parameters corresponding to measured (real) conditions within waveguide match each other as close as possible (Kolarski et al. 2023, Kolarski et al. 2023b).

Modelling procedure was designed both for unperturbed and perturbed conditions, as best fitting as possible to real measured data using pairs of parameters sharpness β (km⁻¹) and reflection height H' (km) modelled for day time ionospheric conditions (Wait and Spies 1964), providing good agreement between real and modeled data.

Numerical simulations conducted in this research revealed electron density increases of several orders of magnitude during maximal impact of analyzed solar flare events compared to unperturbed ionospheric conditions. Estimated electron densities N_e (m⁻³) at arbitrary height of 74 km are as follows: $2.06 \cdot 10^{11}$ m⁻³, $1.15 \cdot 10^{12}$ m⁻³, $1.76 \cdot 10^{10}$ m⁻³ and $2.12 \cdot 10^{11}$ m⁻³ in cases of X2.2, X9.3, X1.4 and X8.2, respectively. In case of strongest of SFs analyzed, this is almost 4 orders of magnitude higher compared to unperturbed value of $2.16 \cdot 10^8$ m⁻³ at the same reflection height. Electron densities related to maximal impact of high class X-ray SFs from September 2017, estimated at arbitrary height of 74 km, obtained according to conducted numerical modeling procedure are given in function of X-ray soft solar flux in Figure 3, indicated by black stars. Best fitting to general trend

obtained from numerous previous studies based both on data recorded in Belgrade and from other research groups worldwide dealing with VLF technology is obtained for two SFs that occurred on 6th September, one of relatively weak intensity X2.2 and the other with very strong intensity X9.3, the strongest one of cases analyzed here.

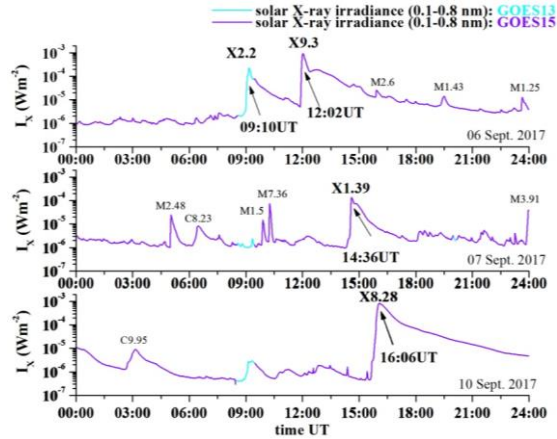


Fig. 1. Solar X-ray irradiance in soft range wavelengths (0.1-0.8 nm) during September 6th, 7th and 10th, 2017 (from upper to lower panel), as reported from GOES15 (violet) and GOES13 (light blue) satellites

Table 1. Solar activity of 24th SC descending branch in relation to X-ray solar flares (sources: NOAA National Centers for Environmental Information and Royal Observatory of Belgium)

year	av. yearly sunspot no.	no. of SF events				
		C-class	M-class	X-class		
2014*	113.3	1779	204	M1-M5=181	16	X1-X5=16
				M5-M9=23		X5-X9=0
2015	69.8	1368	125	M1-M5=115	2	X1-X5=2
				M5-M9=10		X5-X9=0
2016	39.8	320	15	M1-M5=12	/	X1-X5=0
				M5-M9=3		X5-X9=0
2017	21.7	237	39	M1-M5=33	4	X1-X5=2
				M5-M9=6		X5-X9=2
2018	7.0	13	/	M1-M5=0	/	X1-X5=0
				M5-M9=0		X5-X9=0
2019	3.6	32	/	M1-M5=0	/	X1-X5=0
				M5-M9=0		X5-X9=0
2020**	8.8	81	2	M1-M5=2	/	X1-X5=0
				M5-M9=0		X5-X9=0

* 24th SC max.: April 2014 and ** 24th SC min.: September 2020

Table 2. Solar activity during 2017 in relation to X-ray solar flare events (sources: NOAA National Centers for Environmental Information and Royal Observatory of Belgium)

2017	C-class SFs (Σ 237)		M-class SFs (Σ 39)		X-class SFs (Σ 4)		av. monthly sunspot no.
	no.	strength	no.	strength	no.	strength	
January	8	1 – 9.3	/	/	/	/	26.1
February	6	1.1 – 4.1	/	/	/	/	26.4
March	11	1 – 5.1	/	/	/	/	17.7
April	45	1 – 8	7	1.2 – 5.8	/	/	32.3
May	5	1 – 3.3	/	/	/	/	18.9
June	17	1 – 8	/	/	/	/	19.2
July	32	1 – 8.4	3	1.3 – 2.4	/	/	17.8
August	44	1 – 9.4	1	1.1	/	/	32.6
September	68	1 – 9.8	27	1 – 8.1	4	1.3 – 9.3	43.7
October	1	1	1	1.1	/	/	13.2
November	/	/	/	/	/	/	5.7
December	/	/	/	/	/	/	8.2

Table 3. X-class SFs from September 2017, from GOES15 database of soft solar flux component (0.1-0.8 nm)

Solar fare date	Class	$I_{x_{max}}$ Time UT (hh:mm)	$I_{x_{max}}$ (10^{-4} Wm^{-2})
6 th Sept. 2017	X2.2	09:10	2.2658*
6 th Sept. 2017	X9.3	12:02	9.3293
7 th Sept. 2017	X1.3	14:36	1.3880
10 th Sept. 2017	X8.2	16:06	8.2808

* GOES13 data

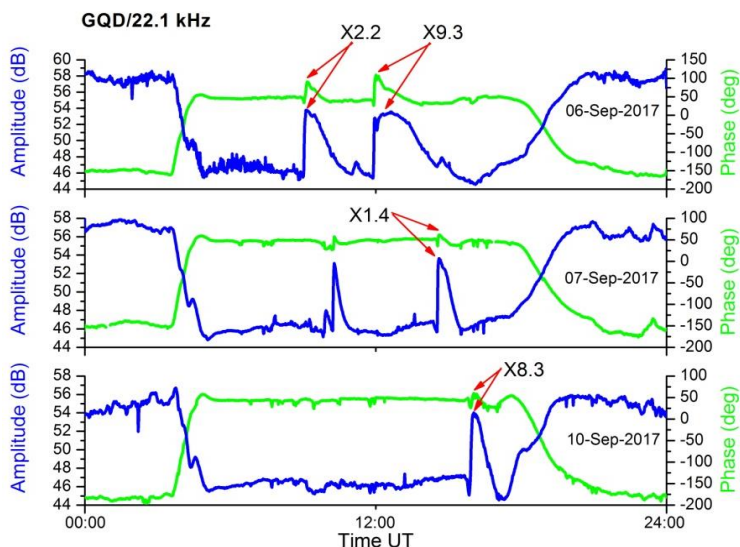


Fig. 2. GQD/22.10 kHz VLF signal perturbed phase (green) and amplitude (blue) during very active days of September 2017: 6th, 7th and 10th (from upper to lower panel) with perturbations related to high class X-Ray SFs indicated by red arrows, recorded by Belgrade VLF station

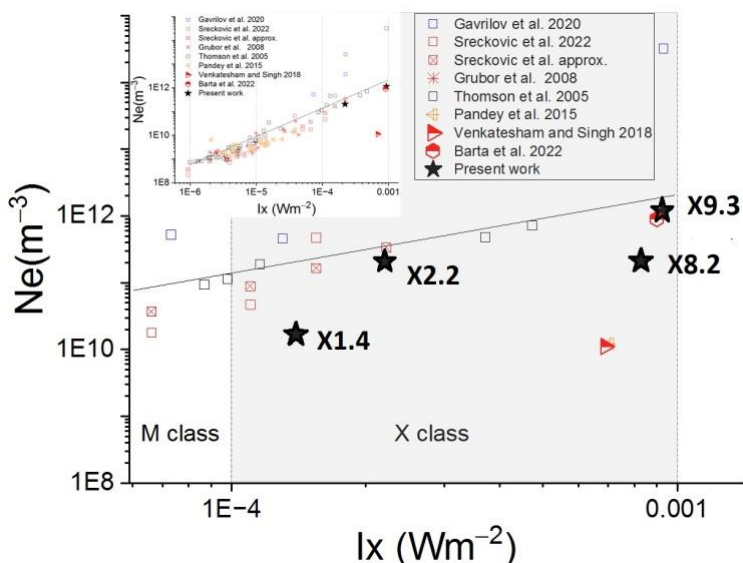


Fig. 3. Estimated electron densities N_e (m^{-3}) at arbitrary height of 74 km (black stars), related to high class X-ray SFs from September 2017, obtained by conducted numerical modeling procedure, in function of X-ray soft solar flux (0.1-0.8 nm) component

Discussion and Conclusions

Influences of high class X-ray SFs, belonging to descending branch of 24th SC, to mid-latitude lower ionosphere over Europe were investigated by employing ground-based technology for remote sensing using VLF signals transmitting within Earth-ionosphere waveguide.

Based on measured VLF signal perturbations registered in Belgrade, Serbia, numerical modeling procedure is conducted in order of retrieving propagation parameters of analyzed VLF signals and ultimately obtaining data related to lower ionospheric parameters under intensely perturbed conditions. Influences of four SF events of X-class from September 2017, as the most active period in terms of solar activity producing high X-class SFs over entire 24th solar cycle, i.e. impact of X1.4, X2.2, X8.2 and X9.3 events to VLF radio signal propagation disturbances monitored on GQD/22.1 kHz signal were analyzed in detail and presented.

During maximal X-ray irradiances of analyzed SF events, observations showed that caused changes in GQD signal amplitude reached up to 8 dB and up to a few tens of degrees in phase, as compared to unperturbed ionospheric conditions. Based on measured data, numerical simulations gave output providing good agreement between real and modeled data. Estimated electron density during perturbed ionospheric states corresponding to maximal impact of analyzed SFs showed increases of several orders of magnitude, as compared to unperturbed ionospheric conditions, with maximal value of $1.15 \cdot 10^{12} \text{ m}^{-3}$ at arbitrary height of 74 km in case of strongest X9.3 SF event.

Investigations of ionospheric responses to energetic solar phenomena, like high class SFs presented in this paper, are not only important for exploration of both magnetospheric plasma properties and ionospheric physics, but also for obtaining deeper insights into and for potential predictions of extreme space weather effects on modern society actions.

Acknowledgments: This work was funded by the Institute of Physics Belgrade, University of Belgrade, through a grant by the Ministry of Science, Technological Development and Innovations of the Republic of Serbia. Author thanks D. Šulić for instrumental set-up.

References

- Appleton, E.V., 1953, *J. Atmos. Terr. Phys.* 3 (5), 282–284.
Barta, V., Natras, R., Srećković, V., Koroncay, D., Schmidt, M., Šulic, D., 2022, *Front. Environ. Sci.*, 10.
Cramer, W., Guiot, J., Marini, K. (Eds.). (2021). *MedECC (2020) Climate and Environmental Change in the Mediterranean Basin – Current Situation and Risks for the Future. First Mediterranean Assessment Report.*

- Eastwood, J.P., Biffis, E., Hapgood, M.A., Green, L., Bisi, M.M., Bentley, R.D., Wicks, R., McKinnell, L.A., Gibbs, M.; Burnett, C., 2017, *Risk Anal.*, 37, 206–218.
- Ferguson, A. J., 1998, Computer program for assessment of long-wavelength radio communications, Version 2.0., Technical document 3030, Space and Naval Warfare Systems Center, San Diego CA 92152-5001, USA.
- Grubor, D., Šulić, D., Žigman, V., 2008, *Ann. Geophys.*, 26, 1731.
- Hayes, L. A., O'Hara, O. S. D., Murray, S. A., Gallagher, P. T., *Sol. Phys.*, 296, 157.
- IPCC, 2023: Summary for Policymakers. In: *Climate Change 2023: Synthesis Report. A Report of the Intergovernmental Panel on Climate Change. Contribution of Working Groups I, II and III to the Sixth Assessment Report of the Intergovernmental Panel on Climate Change.* IPCC, Geneva, Switzerland, 36 pages. (in press).
- Kelly, M. C., 2009, *The Earth's Ionosphere: Plasma Physics and Electrodynamics*, Second Edition.
- Manju, G., Pant, T. K., Devasia, C. V., Ravindran, S., Sridharan, R., 2009, *Ann. Geophys.*, 27, 3853–3860.
- Martinich, J., Crimmins, A., 2019, *Nat. Clim. Chang.* 9, 397–404.
- McRae, W. M., Thomson, N. R., 2004, *J. Atmos. Sol.-Terr. Phys.* 2004, 66, 77–87.
- Riley, P., Love, J.J., 2017, *Space Weather*, 15, 53–64.
- Rycroft, M., Israelsson, S., Price, C., 2000, *J. Atmos. Sol.-Terr. Phys.*, 62, 1563.
- Sahai, Y., Becker-Guedes, F., Fagundes, P.R., Lima, W.L.C., de Abreu, A.J., Guarnieri, F.L., Candido, C.M.N., Pillat, V.G., 2007, *Ann. Geophys.*, 25, 2497–2502.
- Silber, I. & Price, C., 2017, *Surv. Geophys.*, 38(2), 407–441.
- Srećković, V. A., Šulić, D.M., Ignjatović, L., Vujčić, V., 2021, *Appl. Sci.* 11, 7194.
- Thomson, N. R., Rodger, C. J., Clilverd, M. A., 2005, *J. Geophys. Res. Space Phys.*, 110.
- Kolarski, A., Grubor, D., 2014, *Adv. Space Res.*, 53, 1595.
- Kolarski, A., Veselinović, N., Srećković, V.A., Mijić, Z., Savić, M., Dragić, A., 2023, *Remote Sens.*, 15, 1403.
- Kolarski, A., Srećković, V. A., Langović, M., Arnaut, F., 2023, *Contrib. Astron. Obs. Skaln.Pleso.* 2023b, 53, 138-147.
- Wait, R. J., Spies, K. P., 1964, *Characteristics of the Earth-Ionosphere waveguide for VLF radio waves*, NBS Technical Note 300, USA.
- Yasyukevich, Y., Astafyeva, E., Padokhin, A., et al., 2018, *Space Weather*, 16, 1013.
- Žigman, V., Grubor, D., Šulić, D., 2007, *J. Atmos. Sol.-Terr. Phys.* 69, 775–792.
- Šulić, D. M., Srećković, V. A., Mihajlov, A. A., 2016, *Adv. Space Res.*, 57, 1029.

Australian space weather forecasting center: <https://www.sws.bom.gov.au/>.
Center of Excellence in Space Sciences India, IISER Kolkata:
<http://www.cessi.in/spaceweather/about.html>.
ESA Space Weather services: <https://swe.ssa.esa.int/user-domains>.
Geostationary Operational Environmental Satellite (GOES) archive database:
<https://satdat.ngdc.noaa.gov/sem/goes/data/avg/>.
NOAA National Centers for Environmental Information:
<https://satdat.ngdc.noaa.gov/sem/goes/data/avg/>.
WDC-SILSO, Royal Observatory of Belgium, Brussels:
<https://www.sidc.be/SILSO/sunspotbulletin>.
Worldwide Archive of Low-Frequency Data and Observations (WALDO):
<https://waldo.world/>.

Pseudo harmonic oscillator potential

Iacob, F.¹ 

¹West University of Timisoara,
E-mail felix.iacob@e-uvt.ro

It is discussed and shown an analytical results for a chemical potential that can be assimilated to a harmonic oscillator. It can be applied to describe particles that are in a trap created in the plasma medium. Depending on the specificity of the bounding interaction this potential can be modified according to the states of a particle trapped inside. Unlike the classical harmonic oscillator potential, which is an infinitely deep well, the presented potential is tunable and the trapped particle can escape above a certain energy. This model can be used to describe particle trapping, such as electrostatic trapping in plasma. This is an essential effect that should be added to the description of the Dynamics of the plasma fluid and other collective systems. Furthermore, a damped harmonic oscillator can be a successful model to describe the adiabatic cooling process of a trapped atomic/molecular system.

This presentation's goals are to illustrate the potential's analytical construction and demonstrate how its parameters can be changed.

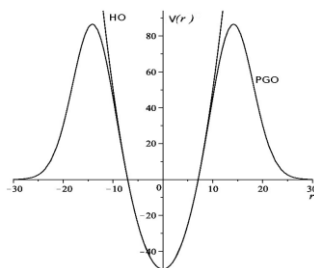


Fig. 1. Pseudo gaussian potential energy curve versus harmonic oscillator

References

- F. Iacob, M. Lute, Exact solution to the Schrödinger's equation with pseudo-Gaussian potential, *J. Math. Phys.* 56 (12), 121501
- F. Iacob, Relativistic pseudo-Gaussian oscillators, *Physics Letters A* 374 (11-12), 1332-1335

Reactive collisions between electrons and molecular cations. Applications in astrophysics and cold plasmas modelling

Pop, N.,¹  Djuissi, E.,² Mezei, J.Z.³  and Schneider, I.F.^{2,4}

¹*Dept. of Fundamentals of Physics for Engineers, Politehnica University Timisoara, Romania*

²*Laboratoire Ondes et Milieux Complexes, CNRS, Univ. le Havre Normandie, France*

³*Inst. of Nuclear Research of the Hungarian Academy of Sciences, Debrecen, Hungary*

⁴*Laboratoire Aimé Cotton, CNRS, ENS Cachan and Univ. Paris-Sud, Orsay, France*

E-mail: nicolina.pop@upt.ro

Dissociative recombination (DR) of molecular cations with electrons is a major elementary process in the kinetics and in the energy balance of astrophysical ionized media (supernovae, interstellar molecular clouds, planetary ionospheres), fusion plasmas in the divertor region, hypersonic entry plasmas and in many other cold media of technological interest.

Using Multichannel Quantum Defect Theory (MQDT), cross sections and Maxwell rate coefficients have been obtained for DR and ro-vibrational transition (RVT) as ro-vibrational excitation (RVE, inelastic collisions), ro-vibrational de-excitation (RVdE, super-elastic collisions) of H_2^+ and HD^+ for numerous ro-vibrational states of the ion. The computational results obtained are in reasonable agreement with experimental data (Motapon et al., 2014; Epée et al., 2016).

A complete set of vibrationally resolved rate coefficients for BeH^+ cation and its isotopomers: BeD^+ , BeT^+ reactive collisions with electrons below the ion dissociation threshold has been provided (Niyonzima et al., 2017; Niyonzima et al., 2018; Pop et al., 2021).




The resulting data are useful for the modeling of the kinetics of the Early Universe and of the magnetic-confinement-fusion-edge plasma.

Our previous studies of DR, vibrational excitation/de-excitation and dissociative excitation (DE) of the BeH^+ ion, based on the MQDT, are extended to collision energies above the dissociation threshold (up to 12 eV) by increasing the number of dissociative states for all molecular symmetries (Djuissi et al., 2024).

References

- O. Motapon N. Pop, F. Argoubi, J. Zs Mezei, M. D. Epee Epee, A. Faure, M. Telmini, J. Tennyson, and I. F. Schneider, *Phys. Rev. A*, 2014, 90, 012706-1-012706-9.
- M. D. Epée, J. Zs Mezei, O. Motapon, N. Pop, I. F. Schneider, *MNRAS*, 2016, 455(1), 276-281.
- S. Niyonzima, S. Ilie, N. Pop, et al., *Atomic Data and Nuclear Data Table*, 2017, 115-116, 287-308.
- S Niyonzima, N Pop, et.al, *Plasma Sources Sci. Technol.*, 2018, 27, 025015(10pp).
- N. Pop, F. Iacob, S. Niyonzima, A. Abdoulanziz, V. Laporta, D. Reiter, I. F. Schneider, *J. Zs Mezei, Atomic Data and Nuclear Data Table*, 2021, 139, 101414(27pp).
- E. Djuissi, J. Boffelli, R. Hassaine, N. Pop, V. Laporta, K. Chakrabarti, M. Ayouz, A. Bultel, J. Zs. Mezei, I. F Schneider, *Physical Chemistry Chemical Physics*, 2024, 26, 18311-18320.

Soft x-ray photoelectron-photoion-photoion coincidence (PEPIPICO) spectroscopy of isolated molecular systems at PLEIADES beamline (SOLEIL synchrotron)

Milosavljevic, A.R.,¹  Nicolas, C.,¹  Robert, E.¹ and Bozek, J.¹ 

¹*Synchrotron SOLEIL, 91190 Saint-Aubin, France*

E-mail: milosavljevic@synchrotron-soleil.fr

The soft X-ray beamline PLEIADES at Synchrotron SOLEIL facility (France) will be presented, with the focus on the energy and angle resolved (Auger) electron - ion coincidence permanent setup (EPICEA). The EPICEA allows for photoelectron-photoion-photoion coincidence (PEPIPICO) and Auger electron-photoion-photoion coincidence (AEPIPICO) spectroscopy (PLEIADES, 2019; Ganguly et al., 2022). The setup consists of a double toroidal electron analyzer (DTA) (Miron et al., 1997) and a 3D focusing ion TOF spectrometer. Electrons emitted at an angle of 54.71° are accepted by the DTA and selected according to their predetermined pass energy (E_p). The detection electron kinetic energy window is about 12% of the defined E_p , whereas the energy resolution is about 1% of the E_p . After exiting the DTA, the electrons are recorded by a delay-line position sensitive detector (DLD40, Roentdek GmbH), where the distance of the electron position from the center is inversely proportional to its kinetic energy. The interaction region is placed in a zero-electric-field space between two extraction grids. The detection of an electron triggers a pulsed field that accelerates the ions toward a hexagonal delay-line detector (HEX75, Roentdek GmbH) placed after the TOF drift tube. The positions on the detector and time of flight of all extracted ions are recorded. Additionally, a pulse generator (Stanford DG645) was used to produce random triggers, which extract ions present in the interaction without a coincident electron event, thus allowing to analyze the background ion signal recorded due to false coincidences. In the present lecture, example results will be presented for several different molecular targets that are interesting for a range of research topics.

References

- PLEIADES Beamline website, <https://www.synchrotronsoleil.fr/fr/lignes-de-lumiere/pleiades>, 2019.
Smita Ganguly et al, Phys. Chem. Chem. Phys., 2022, 24, 28994–29003
Catalin Miron et al, Rev. Sci. Instrum., 1997, 68, 3728–3737.

Neural Networks in Astrophysics and Plasma Physics: Transformers, PINNs, KANNs, and all that

Kouchev, O.¹ and Simeonov, G.¹

¹*Institute of Mathematics and Informatics, Bulgarian Academy of Sciences*
E-mail: kouchev@abv.bg

Recently, new approaches have been developed for the numerical solution of problems in Dynamical systems and boundary value problems for Partial differential equations, which are based on the very general models of the type of Neural networks. Those of them who respect the physical background of the processes are called Physics Informed models (PINNs); their respect to the physics is expressed by means of the properly formulated loss functional which uses explicitly the differential equations and the boundary value conditions in a regularized fashion. Despite not excelling in terms of performance (accuracy and training computing time), PINNs present a compelling alternative for addressing challenges that prove **difficult for traditional methods**, such as inverse problems or parametric partial differential equations (PDEs).

Things have gone much further by trying to mimic in other areas the revolutionary innovation in NLP (especially, in the Large Language models - LLMs) – the so-called Transformers. However, their applicability is still restricted to processes described by Dynamical systems, i.e. where the time is present in the equation.

We will give a short overview of the above newest developments in the area of AI, and to some successful applications to Astrophysics and Plasma Physics.

References

- Hubert Baty, 2024, A hands-on introduction to Physics-Informed Neural Networks for solving partial differential equations with benchmark tests taken from astrophysics and plasma physics, <https://arxiv.org/abs/2403.00599>
- Baty and Vigon, 2024, Modelling solar coronal magnetic fields with physics-informed neural networks, <https://arxiv.org/abs/2310.17919>
- Zhiyuan Zhao, Xueying Ding, B. Aditya Prakash, 2023-2024, PINNsFormer: A Transformer-Based Framework For Physics-Informed Neural Networks, <https://arxiv.org/abs/2307.11833>

Kinetic and fluid studies on Resistive Plate Chambers operated with new eco-friendly gas mixtures

Dujko, S.,¹  Simonović, I.B.¹  and Bošnjaković, D.V.¹ 

¹*Institute of Physics Belgrade, Pregrevica 118, 11080 Belgrade, Serbia*
E-mail: sasa.dujko@ipb.ac.rs

Resistive plate chambers (RPCs) are parallel plate gaseous detectors commonly used for timing and triggering purposes in many high-energy physics experiments. RPCs are employed at CERN-LHC (Large Hadron Collider) experiments due to their excellent time resolution, high-rate capability, and relatively low production cost (Rigoletti et al. 2020). They also play a key role in direct measurements of muons in air showers (Abreu et al. 2018) and in some neutrino observatories (Kumar et al. 2017). RPCs are operated with a gas mixture consisting of $C_2H_2F_4$ (between 90% and 95%), a smaller fraction of *i*- C_4H_{10} (around 5%) and SF_6 (usually between 0.3% and 1%). $C_2H_2F_4$ and SF_6 are well-known greenhouse gases with a global warming potential of respectively 1430 and 22800. The substitution of $C_2H_2F_4$ and SF_6 with environmentally friendly alternatives is one of the major challenges in current RPC technology. $C_2H_2F_4$ can be substituted with either a mixture of $C_2H_2F_4$ and CO_2 , or a mixture of $C_3H_2F_4$ and CO_2 , or eventually a mixture of $C_3H_2F_4$ and He (Rigoletti et al. 2020, Abbrescia et al. 2024). On the other hand, CF_3I , C_4F_7N and $C_5F_{10}O$ were considered as alternatives to SF_6 (Guida et al. 2022). The performance of the detector, including detection efficiency, time resolution, and streamer occurrence, with these gases and mixtures has only been tested experimentally so far. This work presents the first comprehensive modelling study of RPCs that operate with the new generation of environmentally friendly gases and corresponding mixtures.

We approached the problem in three stages. We start by presenting complete and consistent cross-section sets for electron scattering in $C_2H_2F_4$ and $C_3H_2F_4$. A cross-section set for electron scattering in C_3HF_5 is also developed, as this gas could also be considered as an alternative to $C_2H_2F_4$. The accuracy of cross-section sets was tested and validated through a series of comparisons between swarm data calculated using a numerical solution of Boltzmann's equation and Monte Carlo simulation (Dujko et al. 2010), and experimental data obtained under pulsed-Townsend conditions. In particular, kinetic calculations (and experimental measurements) have been performed for a range of gas pressures for each of these gases to determine the energy dependence of three-body attachment.

The second stage involves calculating electron swarm transport coefficients and distribution functions for environmentally friendly gases and mixtures across a

broad range of reduced electric fields. Values of mean energy, drift velocity, diffusion tensor, and rate coefficients for electron attachment and ionization are calculated in various $C_2H_2F_4/CO_2/i-C_4H_{10}/SF_6$ and $C_3H_2F_4/CO_2/i-C_4H_{10}/SF_6$ mixtures. In addition, calculations are performed in the same mixtures where SF_6 is replaced by a proper amount of CF_3I , C_4F_7N , and $C_5F_{10}O$. Critical electric fields are calculated in all considered mixtures, which in turn determine the minimum operating voltages of detectors. The study also examines the direct and indirect effects of electron attachment and ionization on electron drift and diffusion, as well as the occurrence of kinetic phenomena like negative differential conductivity.

The third stage of the research methodology involves fluid modeling of the inception and propagation of streamers in new eco-friendly gas mixtures. We study the development of an electron avalanche and its transition into a streamer discharge under LHC-like conditions. The classical fluid model, which involves drift-diffusion and local-field approximations, is implemented in both axisymmetric and 3D settings in the AMReX environment (Simonović et al. 2024). AMReX is an open-source C++ library for massively parallel block structured adaptive mesh refinement applications (Zhang et al. 2019). AMReX is equipped with geometric multigrid solvers that can solve elliptical differential equations, and it supports MPI and OpenMP parallelization on CPUs as well as parallelization on GPUs. The inception and propagation of positive streamers are simulated by assuming a certain level of background ionization, as accurate models of photoionization for complex RPC gas mixtures are not yet available. We calculate the electron density, densities of positive and negative ions, and electric field as a function of the applied electric field for various eco-friendly RPC gas mixtures. Other streamer properties, such as streamer velocity and streamer radius, are also calculated and discussed.

Acknowledgments: This work is supported by the Science Fund of the Republic of Serbia, Grant No. 7749560, Exploring ultra-low global warming potential gases for insulation in high-voltage technology: Experiments and modelling EGWIn.

References

- Abbrescia et al., 2024, Eur. Phys. J. C 84, 300.
Abreu P., et al., 2018, Eur. Phys. J. C 78, 333.
Dujko S., White R.D., Petrović Z.Lj., Robson R.E., 2010, Phys. Rev. E 81, 046403.
Guida R., Mandelli B., Rigoletti G., 2022, Nucl. Inst. And Methods A 1039, 167045.
Kumar A., et al., 2017, Pramana – J. Phys. 88, 79.
Rigoletti G., Mandelli B., Guida R., 2020, J. Instrum. 15, C11003.
Simonović I., Bošnjaković D., Teunissen J., Dujko S., 2024, Plasma Sources Sci. Technol. 33, 085012.
Zhang W., et al., 2019, J. Open Source Softw. 4, 1370.

Lectures

X-shaped radio galaxy 3C 315

Borka Jovanović, V.,¹  Borka, D.¹  and Jovanović, P.² 

¹*Department of Theoretical Physics and Condensed Matter Physics (020), Vinča Institute of Nuclear Sciences - National Institute of the Republic of Serbia, University of Belgrade, P.O. Box 522, 11001 Belgrade, Serbia*

²*Astronomical Observatory, Volgina 7, P.O. Box 74, 11060 Belgrade, Serbia*
E-mail: vborka@vinca.rs

Abstract

Here we want to investigate X-shaped radio galaxy 3C 315, which is a FR II source, but it lies very close to the FRI/FR II borderline. We used publicly available data from Leahy's atlas of double radio-sources and NASA/IPAC Extragalactic Database (NED) in order to investigate its flux density, as well as the spectral index distribution. We obtained spectral index distributions between the frequencies: 1417 MHz - 2695 MHz and 1646 MHz - 2695 MHz. Our conclusion is that the synchrotron radiation is the dominant radiation mechanism over most of the area of 3C 315. Because of very poor hotspots (i.e. warmspots) we investigated which part of the source represents more active regions. The results of this study would be helpful to understand the evolutionary process of the galaxy 3C 315.

Introduction

DRAGNs are Double Radio sources Associated with Galactic Nuclei. They are clouds of radio-emitting plasma which have been shot out of active galactic nuclei (AGN) via narrow jets. As explained by Leahy (1993), a DRAGN is a radio source containing at least one of the following types of extended, synchrotron-emitting structures: jet, lobe, and hotspot complex.

The most of radiation emitted from AGNs is at radio wavelengths. Some of the radio galaxies has X-shaped, and it is called X-shaped or winged radio galaxies. The origin of the X-shaped radio morphology could be explained using the following possibilities:

- 1) the AGN has undergone two separate epochs of activity. The brighter lobes define the axis of current activity (Merritt and Ekers 2002);
- 2) the radio jets are expanding into an asymmetric medium, causing backflow and producing secondary wings (Leahy and Williams 1984; Capetti 2002);
- 3) the coalescence of two supermassive black holes (SMBH) previously hosted

by a pair of merging galaxies (Gopal-Krishna, Biermann and Wiita 2003).

X-shaped structure characterize pairs of lobes centered on a AGN, where one lobe pair is usually brighter than other (Saripalli et al. 2007).

DRAGN 3C 315 is an X-shaped radio source (it has two sets of double lobes angled with respect to each other). From one hand 3C 315 is a well X-shaped source and example where both lobe pairs have FR-I structure (Saripalli et al. 2007). The host galaxy also has high ellipticity and wings close to the minor axis. This source contains only a weak hotspot (warmspot) in the far-side of the north-western lobe, but on the other hand it would still be classified as an FR-II radio galaxy. It was shown that the host galaxy of 3C 315 (Koff et al. 2000) is highly elongated in the north west - south east direction and accompanied by an elliptical galaxy.

Many authors investigated radio galaxy 3C 315. Northover (1976) presented high-resolution maps of 3C 315 made at Cambridge with One-Mile and 5-km radio telescopes. He find that source consists of two extended components on either side of the central object and that the source has a straight spectrum over a wide frequency range suggesting that electrons are continually being supplied from the central object (Northover 1976).

Hogbom presented observation at 4995 MHz and find that the source 3C 315 is strongly polarized (Hogbom 1979). Leahy and Williams presented maps of 3C 315 at 1.4 GHz (Leahy and Williams 1984). Alexander and Leahy presented intensity images of 3C 315 at 1.4, 1.6 and 2.7 GHz (Alexander and Leahy 1987) and made it publicly available via NED (Leahy, Bridle and Strom 2013). They find that 3C 315 is a very unusual source, both structurally and in its spectral behavior. Leahy, Pooley and Rileyet (1986) also studied polarization of 3C 315. There are also other researchers who investigated radio source 3C 315 (Saripalli et al. 2007; Saripalli and Subrahmanyam 2009; Marecki 2012; Yang 2019).

The prototype of X-shaped (winged) DRAGN: 3C 315

The radio source 3C 315 (cross-identifications: 3C 315; 4C +26.47; PKS 1511+26; B2 1511+26; LQAC 228+026 002) is the prototype X-shaped or winged DRAGN. Wings could be described as a secondary pair of lobes, lying at some angle from the main axis defined by the wormspots and the brighter parts of the diffuse lobes.

Unlike most other cases, there are no true hotspots in either pair of lobes, although there is a modest warmspot about three-quarters of the way to the end of the North North East (NNE) lobe.

From the available online-data, we used Flexible Image Transport System (FITS) data files containing the flux densities in Jy ($1 \text{ Jy} = 10^{-26} \text{ W m}^{-2} \text{ Hz}^{-1}$) of some radio source. We described the structure of FITS format, as well as what is useful for our investigation, in our previous papers (Arsenić et al. 2022; Borka

Jovanović et al. 2023a,2023b,2023c). The observed data are available in *An Atlas of DRAGNs* i.e. the "3CRR" sample of Laing, Riley & Longair (1983). This sample contains not only the FITS files, but it also gives the readers very useful information from the literature on the DRAGNs, with tables and references. There are the Introductory Pages, Description Pages (with full details) and the Listings of individual DRAGNs. Also, we used astronomical database compiled by NASA and IPAC with the information and bibliographic references regarding astronomical objects. These data are provided at: (1) J. P. Leahy, A. H. Bridle & R. G. Strom, *An Atlas of DRAGNs* (2013): <http://www.jb.man.ac.uk/atlas/> (Leahy, Bridle and Strom 2013), and (2) NASA/IPAC Extragalactic Database: <http://ned.ipac.caltech.edu/> (Mazzarella and the NED Team 2002).

We used observations of 3C 315 at three different frequencies, 1417 MHz, 1646 MHz and 2695 MHz (Alexander and Leahy 1987). The calculation method, that we developed, was first published in Borka (2007), and further elaborated in Borka Jovanović (2012) and in Borka Jovanović et al. (2012).

From the observations of 3C 315 at the three frequencies, 1417 MHz (21.2 cm), 1646 MHz (18.2 cm) and 2695 MHz (11.1 cm), we determined the contours which represent the lower boundaries of the source. We found that the minimal fluxes are the following: $S_{v,\min} = 0.0018$ Jy at 1417 MHz, $S_{v,\min} = 0.0020$ Jy at 1646 MHz and $S_{v,\min} = 0.0022$ Jy at 2695 MHz. The areas of 3C 315, with the flux density distributions (in Jy) over these areas, we presented by two-dimensional and three-dimensional plots in Figs. 1 - 3.

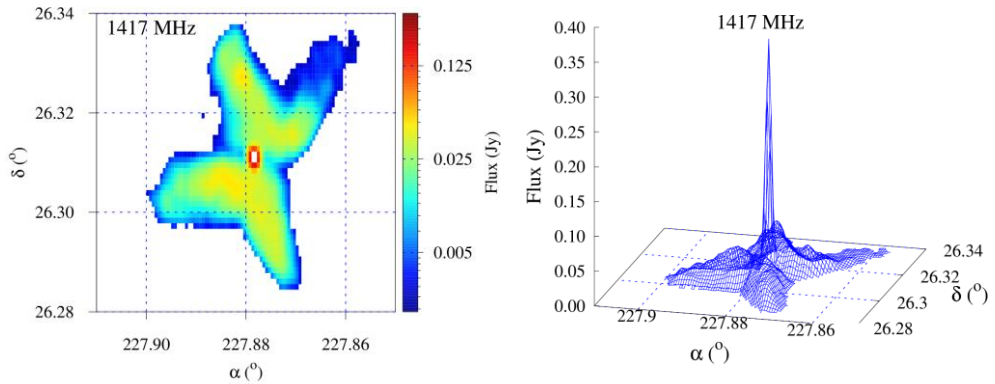


Fig. 1. 2D plot (left) and 3D plot (right) of 3C 315 flux density distribution (in Jy), presented in Equatorial coordinate system (α , δ), at 1417 MHz.

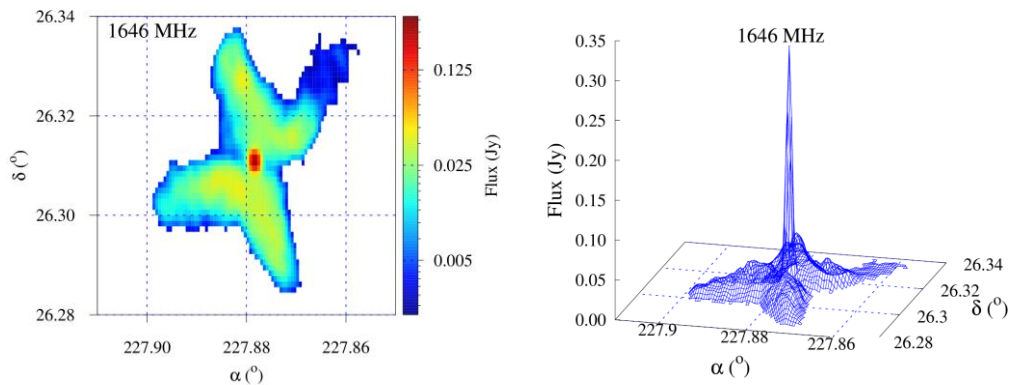


Fig. 2. The same as in Fig. 1, but for 1646 MHz.

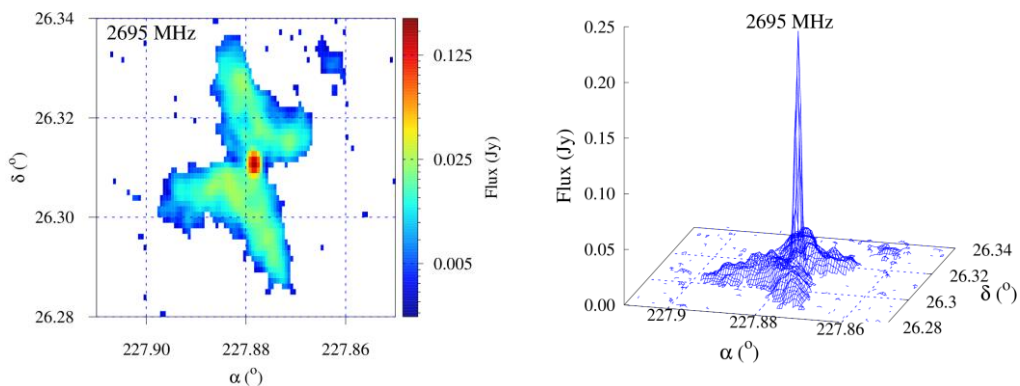


Fig. 3. The same as in Fig. 1, but for 2695 MHz.

Spectral index distribution

The expression which represents the flux density S_ν as a function of frequency ν is given by the expression:

$$S_\nu \sim \nu^{-\alpha}, \quad (1)$$

where α is a constant, called the 'radio spectral index'.

The radio spectral index α can be obtained using the flux density at different frequencies and taking the negative slope of the relation (1). So we calculate it by the following equation:

$$\alpha = -\frac{\log(S_{\nu_1}/S_{\nu_2})}{\log(\nu_1/\nu_2)}. \quad (2)$$

The spectral index is used for classification of radio sources and studying the origin of radio emission:

- If $\alpha > 0.1$ the emission is non-thermal (synchrotron) and it means that it does not depend on the temperature of the source,
- for $\alpha < 0$ it is thermal and depends only on the temperature of the source.

We calculated spectral indices 1417 MHz - 2695 MHz, as well as 1646 MHz - 2695 MHz, over the whole area of 3C 315, and we show how they change over this area in Fig. 4. As expected, these two maps are very similar, because both frequencies 1417 and 1646 MHz (which we combined with 2695 MHz) are very near within the frequency range.

While reading the values of radio spectral index α from the colorbar in Fig. 4, it is noticeable that over the area of 3C 315 it takes values from negative to positive, meaning this: $\alpha > 0$ corresponds to non-thermal mechanism of radiation while $\alpha < 0$ corresponds to thermal mechanism of radiation. For the spectral index of zero value, the flux density is independent of frequency, and the spectrum is said to be flat.

The numerical values of the spectral indices that we have obtained, we further use as a new data. We present it in Fig. 4. The header unit, as well as the part of data unit (table) of this FITS data we show in Fig. 5.

With aim to investigate the distribution of α along some specific directions, we draw the profile lines over the spectral index map 1417 MHz - 2695 MHz (see Fig. 6). The chosen directions, three NNE-SSW and one SE-NW, are the following:

1. $(\alpha, \delta)_{\text{start}} = (227^\circ.8767, 26^\circ.28334)$,
 $(\alpha, \delta)_{\text{end}} = (227^\circ.8867, 26^\circ.33667)$;
2. $(\alpha, \delta)_{\text{start}} = (227^\circ.8733, 26^\circ.28556)$,
 $(\alpha, \delta)_{\text{end}} = (227^\circ.8833, 26^\circ.33889)$;
3. $(\alpha, \delta)_{\text{start}} = (227^\circ.8711, 26^\circ.28667)$,
 $(\alpha, \delta)_{\text{end}} = (227^\circ.881, 26^\circ.33889)$;
4. $(\alpha, \delta)_{\text{start}} = (227^\circ.8639, 26^\circ.31889)$,

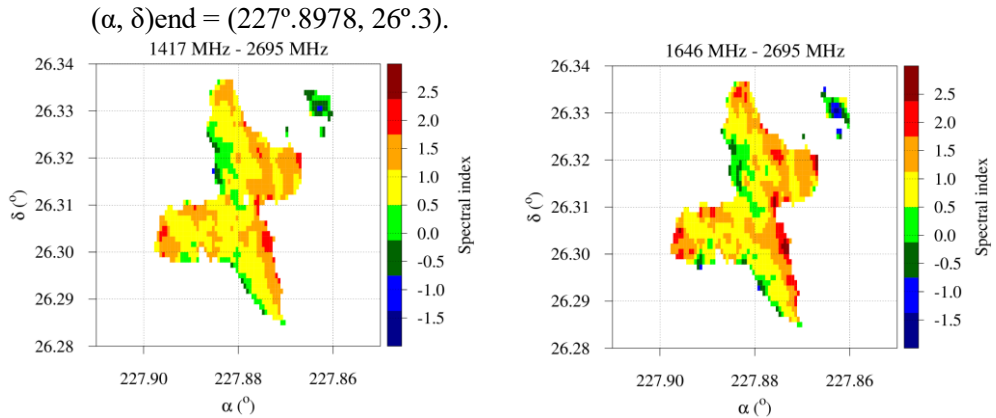


Fig. 4. Spectral indices between 1417 and 2695 MHz (left) and between 1646 and 2695 MHz (right) over the area of 3C 315.

```

SIMPLE = T / file does conform to FITS standard
BITPIX = -64 / number of bits per data pixel
NAXIS = 2 / number of data axes
NAXIS1 = 128 / length of data axis 1
NAXIS2 = 63 / length of data axis 2
EXTEND = T / FITS dataset may contain extensions
COMMENT FITS (Flexible Image Transport System) format is defined in 'Astronomy
COMMENT and Astrophysics', volume 376, page 359; bibcode: 2001A&A...376..359H
CONTENT = 'spectral index' / file contains radio spectral index
CTYPE1 = 'R.A.' / type of data axis 1
CUNIT1 = 'DEG.' / units of data axis 1
CRPIX1 = 1 / reference pixel of data axis 1
CRVAL1 = 227.9139 / coordinate of reference pixel of data axis 1
CDEL1 = -0.0005555556 / increment (pixel size) along data axis 1
CTYPE2 = 'DEC.' / type of data axis 2
CUNIT2 = 'DEG.' / units of data axis 2
CRPIX2 = 1 / reference pixel of data axis 2
CRVAL2 = 26.27667 / coordinate of reference pixel of data axis 2
CDEL2 = 0.0011111111 / increment (pixel size) along data axis 2
ORIGIN = 'P. Jovanovic (AOB)' / origin of FITS file
END
ORIGIN = 'P. Jovanovic (AOB)' / origin of FITS file
    
```

51	0.936519	1.36507	1.45217	1.30404
50	1.02748	1.0823	1.30041	1.30541
49	1.02661	0.754727	1.13401	1.43759
48	0.828574	0.445012	0.646349	1.05074
47	0.521536	0.457455	0.543817	0.685316
46	0.527394	0.519968	0.61764	0.5983
45	1.02868	0.723496	0.615493	0.614627
44	0.547804	0.356786	0.236384	0.48767
43	-0.40605	-0.747602	-0.4701	0.224567
42	-0.118193	-0.931678	-0.748897	-0.068278
41	NULL	-0.285456	-0.226091	-0.00440307
40	NULL	0.57741	0.783228	0.426795
39	-1.1705	0.0464566	0.536583	0.145754
38	-1.33724	-0.304674	0.034094	-0.260995
37	-0.532189	0.183604	0.154719	-0.178641
36	NULL	0.490755	0.111798	-0.308221
35	NULL	1.32645	0.649276	0.00238972

Fig. 5. Header unit (upper part) and a part of data unit (lower part) of the FITS data that we have obtained from our calculated spectral indices over the area of 3C 315.

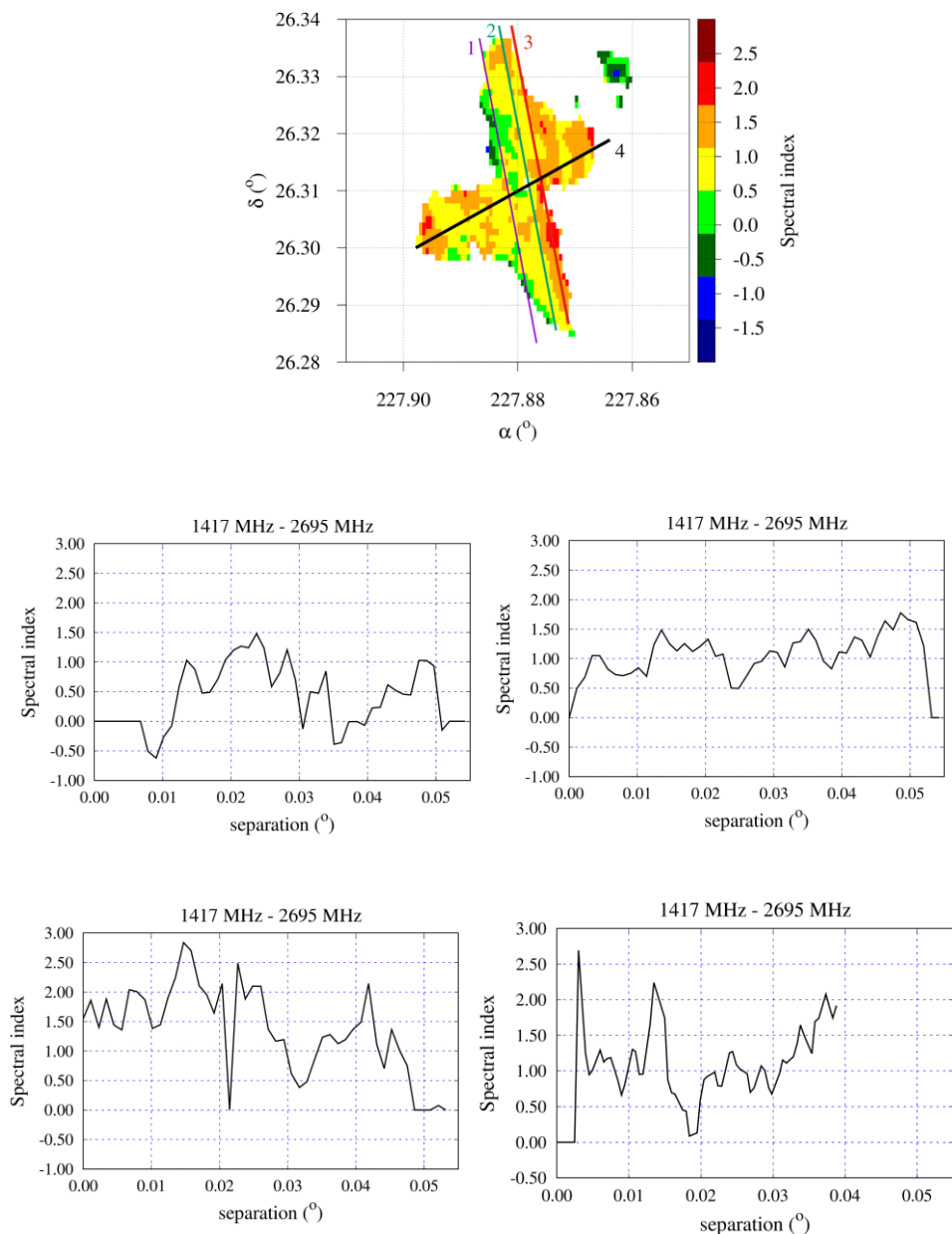


Fig. 6. Spectral index map of 3C 315 between 1417 and 2695 MHz with 4 designated directions: thin purple line, thin green line, thick red line and thick black line. Below map, the four spectral index profiles which correspond to these directions are given.

We can notice that 3C 315 has two pairs of lobes. The direction of the main lobes is NNE-SSW, and that is why we show three profiles along just this direction. Although the spectral index has strong variability over all three studied paths along this direction, nevertheless it can be seen that its average value is different along each of these paths, and that it increases from the first path towards the third one. The first path is taken along valley of spectral indices map, and average value of spectral index along this direction is about 0.5. The second path is parallel to the first one, chosen to connect north-west wormspot and AGN, and has average value of α about 1.1. The third path, also parallel to the first one, and taken along outer border of spectral index map, has average value of α along this direction about 1.5. Therefore, the regions around this third path are with the steepest spectrum along the NNE-SSW direction, meaning that this edge is more recent.

The fourth line is taken along SE-NW axis. The lobes on this axis are not so well defined and are more curved, known as faint extensions of the main lobes i.e. wings. Average value of spectral index along this direction is about 1.1 which is similar to the middle path along the NNE-SSW direction, but variation of spectral indices is much larger than in the previous three cases.

As it can be seen from all four presented profiles, the spectral index is almost always higher than zero, except in only few small parts where it is negative. This indicates that the non-thermal (synchrotron) emission is by far the most dominant radiation mechanism over the whole source.

Also, 3C 315 contains pronounced and bright radio core (see Figs. 1 - 3), but only a weak hotspots. The outer structure is relaxed.

Discussion and conclusions

We used the available flux densities of 3C 315 at 1417, 1646 and 2695 MHz. We provide the spectral index distribution derived between two frequencies: 1417 and 2695 MHz, as well as between 1646 and 2695 MHz. At all three frequencies the flux structure is characterized with no obvious hotspots and the core dominates the flux density distribution. It is noticeable from the spectral index map that this tendency is even more pronounced. We clearly show here that the synchrotron radiation is the dominant emission mechanism over the majority of the area of this radio galaxy.

Some authors propose that X-shaped radio sources may be the result of a few possibilities (Leahy and Williams 1984; Capetti 2002; Merritt and Ekers 2002; Gopal-Krishna, Biermann and Wiita 2003):

- 1) the AGN has undergone two separate epochs of activity (the brighter lobes define the axis of current activity),
- 2) recent collision or merger between two supermassive black holes, which can produce the extra set of jets and lobes;
- 3) the main jets expanded into an asymmetric medium, and in that way

generating an additional pair of radio lobes.

We are led to the conclusion that results of this study will be helpful for understanding the evolutionary process of the 3C 315 radio source. Due to the fact that the host galaxy of 3C 315 (Koff et al. 2000) is accompanied by an elliptical galaxy and both of which are located inside a cluster (an anisotropy in the gas environment is related to the ellipticity of the host galaxy), probably the environment plays the most significant role in the evolution of this object.

Acknowledgments: This work is supported by Ministry of Science, Technological Development and Innovations of the Republic of Serbia through the Project contracts No. 451-03-66/2024-03/200017 and 451-03-66/2024-03/200002.

References

- Alexander, P., Leahy, J. P., 1987, *Mon. Not. R. Astron. Soc.*, 225, 1
- Arsenić, A., Borka, D., Jovanović, P., Borka Jovanović, V., 2022, *Publ. Astron. Obs. Belgrade*, 102, 265
- Borka, V., 2007, *Mon. Not. R. Astron. Soc.*, 376, 634
- Borka Jovanović, V., 2012, *Publ. Astron. Obs. Belgrade*, 91, 121
- Borka Jovanović, V., Borka, D., Skeoch, R., Jovanović, P., 2012, *Publ. Astron. Obs. Belgrade*, 91, 255
- Borka Jovanović, V., Borka, D., Arsenić, A., Jovanović, P., 2023a, *Adv. Space Res.*, 71, 1227
- Borka Jovanović, V., Borka, D., Jovanović, P., 2023b, *Contrib. Astron. Obs. Skalnaté Pleso*, 53, 188
- Borka Jovanović, V., Borka, D., Jovanović, P., 2023c, *PoS BPU11*, 043
- Capetti, A. et al., 2002, *Astron. Astrophys.*, 394, 39
- de Koff, S. et al., 2000, *Astrophys. J. Suppl. Series*, 129, 33
- Gopal-Krishna, Biermann, P. L., Wiita, P. J., 2003, *Astrophys. J.*, 594, L103
- Hogbom, J. A., 1979, *Astron. Astrophys. Suppl.*, 36, 173
- Laing, R. A., Riley, J. M., Longair, M. S., 1983, *Mon. Not. R. Astron. Soc.*, 204, 151
- Leahy, J. P., 1993, "DRAGNs", in *Proceedings: Jets in Extragalactic Radio Sources*, Eds. Roser, H.-J. and Meisenheimer, K., *Lecture Notes in Physics*, 421, 1
- Leahy, J. P., Williams, A. G., 1984, *Mon. Not. R. Astron. Soc.*, 210, 929
- Leahy, J. P., Pooley, G. G., Riley, J. M., 1986, *Mon. Not. R. Astron. Soc.*, 222, 753
- Leahy, J. P., Bridle, A. H., Strom, R. G., 2013, *An Atlas of DRAGNs* - online: <http://www.jb.man.ac.uk/atlas/>
- Marecki, A., 2012, *PoS RTS2012*, 24
- Mazzarella, J. M. and the NED Team, 2002, "Using the NASA/IPAC Extragalactic

- Database (NED) and Federated Virtual Observatory Archives for Multiwavelength Studies of AGN”, in Proceedings: AGN Surveys, Eds. Green, R. F., Khachikian, E. Ye. and Sanders, D. B., Astron. Soc. Pacific Conference Series, 284, 379
- Merritt, D., Ekers, R. D., 2002, *Science*, 297, 1310
- Northover, K. J. E., 1976, *Mon. Not. R. Astron. Soc.*, 177, 307
- Saripalli, L., Subrahmanyan, R., Laskar, T., Koekemoer, A., 2007, *PoS MRU*, 130
- Saripalli, L., Subrahmanyan, R., 2009, *Astrophys. J.* 695, 156
- Yang, X., Joshi, R., Gopal-Krishna, An, T., Ho, L. C., Wiita, P. J., Liu, X., Yang, J., Wang, R., Wu, X.-B., Yang, X., 2019, *Astrophys. J. Suppl.* 245, 17

Study of very thin crystals by rainbow scattering effect

Starčević, N.¹  and Petrović, S.¹ 

*Institute of Nuclear Sciences - National Institute of the Republic of Serbia,
University of Belgrade, P.O. Box 522, 11001 Belgrade, Serbia
E-mail: nikolas@vin.bg.ac.rs*

Abstract

This research introduces an innovative methodology for the analysis of very thin crystals, utilizing the rainbow scattering, a technique previously unexploited for this application. The focus is on assessing the capabilities of this method for an in-depth investigation of crystalline structures. To characterize the very thin crystals, we implemented numerical simulation techniques to model and evaluate rainbow scattering phenomena under channeling conditions. The simulations aimed to forecast the scattering patterns of protons as they traversed various cubic crystal types at different orientations. We identified distinct patterns of rainbow scattering, providing essential insights into the internal configurations and orientations of the cubic crystals examined. The combination of channeling mode rainbow scattering with numerical simulations presents a fresh and efficient approach for analyzing very thin crystals, setting the stage for subsequent experimental investigations. This advancement holds considerable promise for enhancing research in the fields of materials science and nanotechnology.

Introduction

Thin crystal characterization is a crucial field in materials science, particularly in the study of thin films and nanostructures. Over the years, a variety of techniques have been employed to characterize thin crystals, each providing valuable insights into the material's structure and properties (Benz 2014). Ion channeling stands out as a powerful technique for studying the internal structure of crystalline materials (Robinson 1963). When particles pass through a well-aligned crystal, they are "channeled" by the potential well created by the atomic lattice (Gemel 1974). In this process, if the crystal is sufficiently thin, the ions will be transmitted, and each ion preserves its unique spatial and angular information, providing detailed insights into the channeled trajectories. The challenges of analyzing angular distributions of channeled ions through thin crystals can be

easily and effectively overcome by applying the crystal rainbow theory (Petrović 2000). In the case of channeling, the scattering angles of ions exhibit distinct features and are constrained within specific values known as rainbow lines. This effect arises due to the singularity of the classical differential cross-section in ion scattering. The rainbow lines in the transmission angle (TA) plane are comparable with the angular distribution of channeled ions. Crystal rainbow theory accurately predicts the spatial and angular distributions of ions channeled through crystals.

Experimental proof of crystal rainbow theory was conducted in a high-resolution ion transmission channeling experiment (Motapothula 2012). Detailed analysis of crystal rainbow theory led to the correction of the ion-crystal interaction potential in the case of channeling (Petrović 2015). Based on these results, we constructed interaction potentials for other cubic crystals (Petrović 2019, Starčević 2021, 2023). Also influence of crystal electrons on channeled ions is determined (Starčević 2023). The "doughnut effect" which occurs when the ion beam is tilted away from a major crystallographic direction, was theoretically explained using crystal rainbow theory in interpretation of experimental results of angular distributions of channeled protons as the crystal tilting angles increase (Motapothula 2012). Applications of rainbow scattering for theoretical analysis of graphene sheets have led to the determination of several physical quantities, (Ćosić 2019, 2021, Hadžijojić 2021, 2023).

One of the remarkable features of rainbow lines is that by analyzing angular distributions of channeled ions, which are completely determined by the shape of rainbow lines, it is possible to determine the shape of the crystal channel. As the image of rainbow lines in the impact parameter (IP) plane lie within the channel region where the contributions of all atomic strings defining the channel are significant this line will be "repelled" by the atomic strings defining the channel, and the coordinates of its points are solely determined by the arrangement of the atomic strings. This means that the angular distributions of transmitted ions can be described, since rainbow lines in the TA plane appear as their "skeleton". Further on, unknown crystal thickness is indicated by the reduced thickness parameter Λ (Krause 1994), which represents the crystal thickness in terms of the wavelength for the projectile's transverse oscillating motion $\Lambda = f(q, m_p)L/v$, where L is the crystal thickness, v is the projectile speed, and f is the transverse oscillation frequency of the projectile, q and m_p are its charge and mass. The evolution of the angular distributions with the increase of L can be precisely tracked using the reduced crystal thickness, so the evolution of rainbow lines can also be tracked using this variable. By considering crystal rainbow theory and the scaling law, it is possible to determine the type and thickness of a very thin crystal based on the recorded rainbow lines, provided the energy and charge of the projectile are known. Given these factors, we opted to use protons with energy in the MeV range, as we already have experience analyses with these projectiles (Motapothula 2012).

Analysis and results

We are investigating the scattering patterns of 2 MeV protons channeled through very thin cubic crystals in major crystallographic orientations. The main criterion for analysis is that all crystals are considered very thin. With body-centered cubic (BCC), face-centered cubic (FCC), and diamond cubic lattices, including vanadium, chromium, iron, niobium, molybdenum, barium, europium, tantalum, tungsten, aluminum, calcium, nickel, copper, strontium, rhodium, palladium, silver, cerium, ytterbium, iridium, platinum, gold, lead, thorium, silicon, germanium and tin crystals are investigated. The main morphological difference between these three types of cubic crystals lies in the number and position of atoms in the primitive lattice, as shown on Fig. 1.

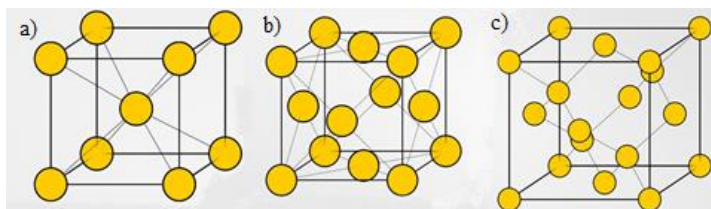


Fig. 1. Primitive lattice of: a) BCC, b) FCC and c) diamond crystals

The differences in the arrangement and positions of atoms in crystal lattices determine the channel shape and positions of its atomic strings. Fig. 2 shows square channels in (001) orientation and hexagonal channels in (111). In FCC crystals, the channel side length will be smaller by a factor of $\sqrt{2}$ compared to that of BCC, and for diamond cubic crystals, the channel will have a side length half that of BCC crystals. Since the shapes of the channels presented in Fig. 2 a), b), and c), d) are completely different, a simple morphological comparison of the rainbow lines can determine the crystal orientation in question. However, a limitation of this morphological approach is that we cannot definitively identify the crystal type based solely on the shape of the rainbow line.

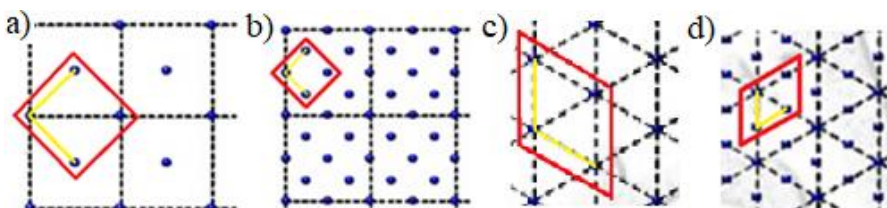


Fig. 2. a) BCC (001), b) diamond (001), c) BCC (111), d) diamond (111) channels

In Fig. 3, the primary rainbow lines of protons channeled through a) square (001) and b) hexagonal (111) channels are presented. The proton energy, crystal

type, and thickness are chosen such that only the primary rainbow line appears in this theoretical representation. Square channel exhibit inner rainbow lines shaped like a cusped square, with the cusps pointing toward the angular positions of the atomic strings defining the channel. In contrast, all hexagonal channels will generate rainbow lines resembling a symmetrical six-pointed star, composed of two cusped equilateral triangles oriented opposite each other. Solely based on the shape of these lines, we can conclude what crystal channel is in question. Thus, we can conclude that the shape of the primary rainbow line allows us to determine the orientation of an unknown crystal.

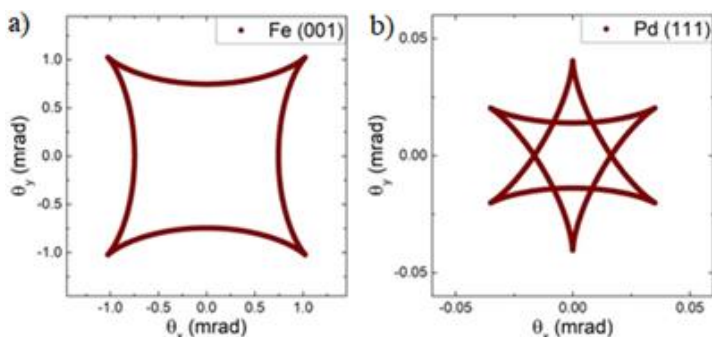


Fig. 3. Shape of rainbow lines for a) square and d) hexagonal channel

As is known, the size of the rainbow line depends on the interaction potential, which is a function of the crystal atomic number and the impact parameter (size of the channel). If we change (gradually reduce) the projectile energy in comparison to the first part of our analysis at some point, a secondary or outer rainbow line will emerge in the area surrounding the atomic strings in the IP plane, and its image will appear in the TA plane. The outer rainbow line will be highly sensitive to the atomic number of the crystal and will not be as sensitive to the influence of all atomic strings and their spatial positions. By measuring the angular distributions of channeled protons and comparing them to the rainbow lines - now consisting of one inner (primary) rainbow line and one outer (secondary) rainbow line - we can conduct a similar morphological analysis to identify the unknown crystal.

In Fig. 4, we present the experimental angular distribution of 2 MeV protons channeled through the (001) channel of a 55 nm thin silicon crystal, along with the calculated rainbow lines in the TA plane and the corresponding rainbow lines in the IP plane. This combination of crystal thickness and proton energy yields a reduced crystal thickness less than 0.25, so the silicon crystal can be considered very thin.

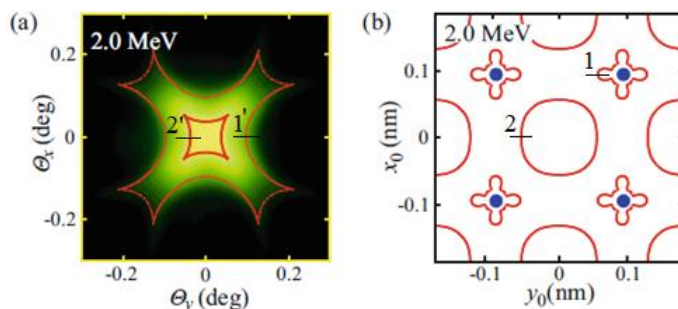


Fig. 4. a) Proton experimental angular distributions with rainbow lines, b) corresponding rainbow lines in the IP plane

Based on these results, we conducted an analysis of all cubic crystals in the (001) orientation. Our goal is to, by calculating the angular position of the outer rainbow line, deduce the atomic number of the crystal. We specifically calculated the positions of the outer rainbow lines along position 1 on Fig. 4, and determined its position 1' in the TA plane. From Fig. 5 a) we can see that as the atomic number of crystal increases, the position of the outer rainbow line in the TA plane exhibits a growing trend. Thus, by measuring this position, we can deduce which crystal is being analyzed. However, some minor flaws in this morphological methodology arise from the fact that some crystals have similar ratio of atomic number and channel size. This leads to a slight indeterminacy when distinguishing between these elements.

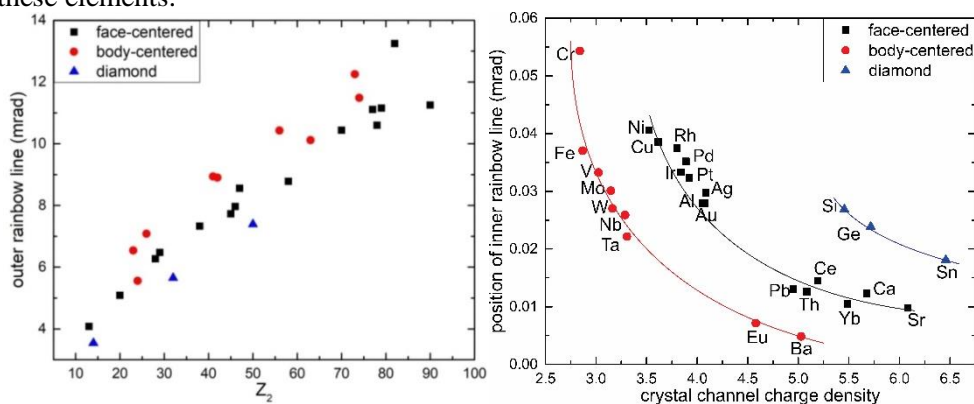


Fig. 5. Positions of a) outer rainbow lines, b) inner rainbow lines

However, if we consider the physical parameters that differentiate these crystals - such as channel area, thickness of one layer, crystal atomic number - and compare them with the positions of the inner rainbow lines for all these types of cubic crystals, as presented in Fig. 5 b), some ambiguities will be clarified. The surface charge density per crystal channel is defined as the ratio of the atomic number of the crystal to the number of atomic strings defining the crystal channel. This

approach allows us to overcome the morphological differences between the three types of cubic crystals, specifically addressing the total number of atoms in one crystal lattice as seen in cross-section for each different orientation. For all analyzed cubic crystals in the (001) orientation, the number of atomic strings per primitive crystal lattice is five for BCC crystals, nine for FCC crystals, and thirteen for diamond cubic crystals. This allows us to categorize these cubic crystals into three distinct groups, as illustrated in Fig. 5 b). All crystals with a BCC structure are fitted along the red line, those with a FCC structure along the black line, and diamond crystals are fitted along the blue line. Notably, while some elements may have similar positions for their outer rainbow lines, they can be easily distinguished by considering the morphological position of their inner rainbow line, making it straightforward to sort them based on these values. This way total separation of the different elements is achieved, with the main criterion that the crystal is considered very thin.

Conclusions










We applied crystal rainbow theory to characterize various cubic crystals. Our findings underscore the potential of using crystal rainbow theory as a powerful tool for the characterization of thin crystals. We demonstrated that the morphology of rainbow lines provides a reliable means to determine the orientation of unknown thin crystals. Our analysis revealed distinct differences in the shapes of channels and their corresponding rainbow lines across different orientations. We also showed that the position of the secondary rainbow line can be effectively used to distinguish between different crystals, as its position increases with the atomic number of the crystals. We introduced the concept of charge density per crystal channel, which allowed us to categorize the cubic crystals using inner rainbow line into three distinct groups, each corresponding to a different type of cubic crystal. Overall, our findings underscore the potential of using crystal rainbow theory as a powerful tool for the morphological characterization of thin crystals. Future studies could focus on extending this methodology to other crystals, thereby broadening its applicability and enhancing our understanding of ion channeling phenomena.

References

- Benz K. W., Neumann W., Mogilatenko A., 2014, *Introduction to Crystal Growth and Characterization*, Wiley
- Ćosić M. et al., 2019, *Carbon* 145, 161
- Ćosić M. et al., 2021, *Chaos* 31, 093115
- Gemmell D. S., 1974, *Rev. of Mod. Phys.*, 46, 129
- Hadžijojić M. et al., 2021, *J. Phys. Chem. C*, 125, 21030
- Hadžijojić M., Ćosić M., 2023, *Eur. Phys. J. D*, 77, 86

- Krause H.F. et al., 1994, Phys. Rev. A, 49, 283
Motapothula M. et al., 2012, Nucl. Instrum. Methods Phys. Res. B, 283, 29
Motapothula M. et al., 2012, Phy. Rev. B, 86, 205426
Petrović S., Miletić L., Nešković N., 2000, Phy. Rev. B, 61, 1, 184
Petrović S. et al., 2015, Nucl. Instrum. Methods Phys. Res. B, 360, 23
Petrović S. et al., 2019, Nucl. Instrum. Meth. Phys. Res. B, 447, 79
Robinson M. T., Oen O. S., 1963, Appl. Phys. Lett. 2, 30
Starčević N. et al., 2021, Nucl. Inst. Methods Phys. Res. B, 499, 39
Starčević N., Petrović S., 2023, Eur. Phys. J. D, 77, 61
Starčević N., Petrović S., 2023, Nucl. Tech. and Rad. Prot., 38, 3, 162

Implications of the Temperature Effect Analysis Using Simulated Secondary Cosmic Muon Data

Savić, M.R.,¹  Veselinović, N.B.,¹  Dragić, A.L.,¹  Maletić, D.M.,¹ 
Joković, D.R.,¹  Banjanac, R.M.,¹  Knežević, D.,¹  Travar, M.¹  and
Udovičić, V.I.¹ 

¹*Institute of Physics Belgrade, Pregrevica 118, 11080 Belgrade, Serbia*
E-mail: msavic@ipb.ac.rs

As it propagates through the atmosphere, the muon component of secondary cosmic rays is influenced by variations in atmospheric parameters. The two most significant atmospheric effects affecting the muon flux detected at ground level are the barometric effect, due to changes in atmospheric pressure, and the temperature effect, caused by fluctuations in atmospheric temperature.

To enhance the sensitivity of ground-based muon detectors to cosmic ray variations of non-atmospheric origin, these effects must be corrected, with the temperature effect being more complex to model. The most well-established method for correcting the temperature effect is the integral method, based on the theory of atmospheric effects (Dorman 2004). However, as it is not so straightforward to implement, several empirical methods have been developed over the years, including the effective level of generation method (Duperier 1949), the mass-averaged temperature method (Dvornikov et al. 1976), as well as more recent approaches based on principal component analysis (Savić et al. 2019) and machine learning applications (Savić et al. 2021).

Each theoretical and empirical approach has its advantages and limitations, and directly comparing the effectiveness of these methods with real measured data is not necessarily simple. One way to address this is to test model performance on simulated data, where atmospheric variation is the only source of flux change. Preliminary results from data simulated with the CORSIKA package (Heck et al. 1998) provide a clearer picture of the strengths and limitations of these methods. Specifically, the results suggest that the integral method may lead to overcorrections if applied too directly, an issue that hadn't been that obvious before.

References

Dorman, L., Cosmic Rays in the Earth's Atmosphere and Underground. 10.1007/978-1-4020-2113-8. (2004).

- Duperier A., The meson intensity at the surface of the earth and the temperature at the production level, Proceedings of the Physical Society. Section A 62 (11) (1949) 684.
- V. Dvornikov, Y. Y. Krest'yannikov, A. Sergeev, Determination of the variation of average-mass temperature of the atmosphere by data of cosmic ray intensity., Geomagnetism and aeronomy 16 (1976) 923–925.
- M. Savić, A. Dragić, D. Maletić, N. Veselinović, R. Banjanac et al., A novel method for atmospheric correction of cosmic-ray data based on principal component analysis, Astropart.Phys. 109 (2019), 1-11.
- Savić, M., Maletić, D., Dragić, A., Veselinović, N., Joković, D., Banjanac, R., et al. (2021). Modeling meteorological effects on cosmic ray muons utilizing multivariate analysis. Space Weather, 19, e2020SW002712.
- Heck, D.; Knapp, J.; Capdevielle, J. N.; Schatz, G.; Thouw, T., CORSIKA: a Monte Carlo code to simulate extensive air showers. Forschungszentrum Karlsruhe GmbH, Karlsruhe (Germany)., Feb 1998, V + 90 p., TIB Hannover, D-30167 Hannover (Germany).

New opportunities for COST participants – actions networking tools and examples of the national funding schemes

Mijić, Z.R.¹  and Marinković, B.P.¹ 

¹*Institute of Physics Belgrade, Pregrevica 118, 11080 Belgrade, Serbia*
E-mail: zoran.mijic@ipb.ac.rs

As the oldest intergovernmental funding organization in Europe COST (the European Cooperation in Science and Technology) facilitates networking among academics and innovators in order to increase Europe's ability to address scientific, technical, and societal concerns (Marinković and Mijić 2022). According to the study (Seeber et al., 2022a), participation in COST program considerably increases researchers' scientific co-publications, therefore advancing their professional careers. The findings demonstrate a 55% average increase in co-publications among active COST action participants as compared to the proposed network of the researchers of non-founded actions. This increase in collaborative co-publications is not at the expense of non-collaborative ones, resulting in a net gain in scientific production. Keeping in mind that the impact of the actions lasts beyond their lifetime, involvement in COST networking activities significantly improves researchers' productions and experience thus increasing their capacity for long-term collaborations (Seeber et al., 2022b). This is especially important for early-career researchers, as around 42% of COST action members in 2023 are young researchers. (Mijić and Marinković, 2024a).

Over the last several years running the COST action have become more and more competitive (Mijić and Marinković, 2024b). The reported success rate of the action proposals for the last open call OC-2023-1 was 11.5%. Since there is a clear benefit of scientific community involved in research network, several European countries established additional national funding to support research projects originating from successful ongoing COST Actions.

In this study, within proposed mini-project, we will discuss the new opportunities for COST participants through the actions networking tools focusing on young researchers' and ITC (Inclusiveness Target Countries) conference grants entering into force in November 2024. In addition, new technical annex, evaluation grid and introduction of the acceptability criterion for new action proposal will be demonstrated. Finally, the existing opportunities for additional funding of research projects originating from COST actions will be introduced. The recent experience

and good practices of national funding schemes for COST participants in several countries will be presented together with available funding support for COST related projects in Switzerland which include project partners abroad.

Acknowledgements: Thanks are due to The Ministry of Science, Technological Development and Innovation of the Republic of Serbia and the Institute of Physics Belgrade for national COST office support.

References

- Marinković, B., Mijić, Z., 2022, V Meeting on Astrophysical Spectroscopy - A&M DATA - Astronomy & Earth Observations, Book of Abstracts and Contributed Papers, Eds: Vladimir A. Srećković, Milan S. Dimitrijević, Aleksandra Kolarski, Zoran R. Mijić and Nikola B. Veselinović, p.55.
- Seeber, M., Vlegels, J., Seeber, M., 2022a, 26th International Conference on Science and Technology Indicators, Proceedings, Eds: N. Robinson-Garcia, D. Torres-Salinas, W. Arroyo-Machado, sti2239
- Seeber, M., Vlegels, J., Cattaneo, M., 2022b, *J. Assoc. Inf. Sci. Technol.* 73, 1106
- Mijić, Z., Marinković, B., 2024a, Building bridges between climate science and society through a transdisciplinary network, Book of Abstract and Contributed Papers, Eds: Vladimir A. Srećković, Aleksandra Kolarski, Filip Arnaut, and Milica Langović, pp. 89-91.
- Mijić, Z., Marinković, B., 2024b, VI Conference on Active Galactic Nuclei and Gravitational Lensing, Book of Abstract, Eds: J. Kovačević Dojčinović, and V. A. Srećković pp. 34-35.

Posters

Terminator variations of VLF/LF amplitudes - observational techniques and case studies

Eichelberger, H.,¹ Nina, A.,²  Boudjada, M.Y.,¹ Kolarski, A.,² 
Veselinović, N.B.,²  Nico, G.,³  Biagi, P.F.,⁴  and Srećković, V.A.² 

¹*Space Research Institute, Austrian Academy of Sciences, Schmiedlstrasse 6, 8042 Graz, Austria*

²*Institute of Physics Belgrade, University of Belgrade, Pregrevica 118, 11080 Belgrade, Serbia*

³*Institute of Applied Mathematics, Italian National Research Council, Via Giovanni Amendola 122/I, 70126 Bari, Italy*

⁴*Department of Physics, University of Bari, Via Amendola 173, 70125 Bari, Italy*
E-mail: hue@oeaw.ac.at

Abstract

The VLF/LF Earth-ionosphere waveguide enables the remote detection of important variabilities related to environmental and solar processes. Two case studies have been considered with medium and high solar activities, both recorded by Belgrade (Serbia) and Graz (Austria) stations. This study shows the existence of electric field amplitude wave phenomena with periods of ~500 sec during terminator times. Our findings underscore the importance of measurement networks for future surveys.

Introduction

Remote sensing of the lower ionosphere via very low frequency (VLF, $f = 3\text{-}30$ kHz) and low frequency (LF, $f = 30\text{-}300$ kHz) signals emitted by powerful transmitter stations and detected by ground-based facilities are crucial for the study of the Earth's environment, e.g., space weather studies, the coupling between atmosphere and ionosphere, and commercial applications. The radio waves from narrowband VLF/LF transmitters are confined within the Earth-ionosphere waveguide, between the Earth's surface (lower boundary) and the lower ionospheric layers (upper boundaries), i.e., D-layer (altitudes approx. 50-70 km) during daytime, E-layer (altitudes approx. 70-90 km) during night time, and during sunrise and sunset transitions. The ion production in the lower ionospheric D-region is dominated by solar Lyman-alpha (mainly $[\text{NO}^+]$ and cluster ions), to a

minor extend by EUV, UV, X-ray (solar flare events) on the species $[O_2, N_2]$ and at lower altitudes by galactic cosmic rays $[N_2, O_2]$. The D-region electron density profiles show a solar zenith angle dependence as reported in several models (Nina et al., 2021; Friedrich et al., 2018; Mironova et al., 2015; and Wait and Spies, 1964).

VLF/LF observations recorded by Belgrade (Serbian) and Graz (Austria) Stations

In this study we consider two VLF/LF receivers, located in Belgrade (Serbia) and Graz (Austria) as displayed in Figure 1. Table 1 lists the transmitter signal detected by Belgrade and Graz facilities and the corresponding features: frequency, geographical coordinate, and the distances. The reception systems in Belgrade (Nina, 2024) and in Graz (Galopeau et al., 2023) are capable of measuring amplitudes and phases of electric fields with a high time resolution (sampling frequencies f_s 1 sec). Electric fields are associated with transmitter signals propagating in the Earth-ionosphere waveguide. The selected paths shall have a distance far and close to the transmitter station to avoid near field evanescent modes and to enhance the signal-to-noise ratio.

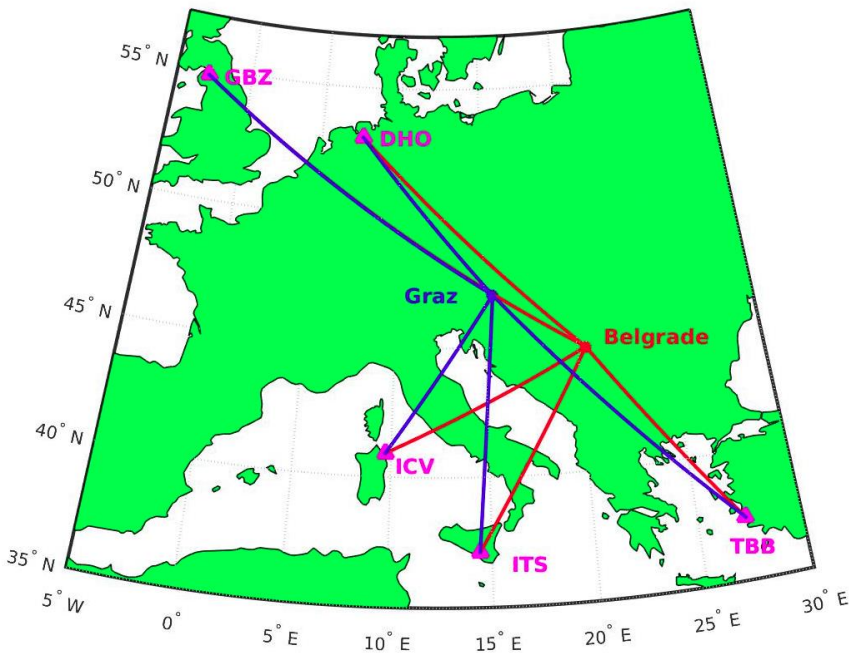


Fig. 1. Geographical locations of the five transmitter signals (i.e., DHO, GBZ, ICV, ITS and TBB) detected by VLF reception systems in Belgrade (Serbia) and Graz (Austria).

Table 1. Great circle path (GCP) distances between Belgrade or Graz reception systems and VLF/LF transmitters (see Figure 1) with fully developed waveguide modes and sufficient S/N ratio.

	ICV 20.27 kHz 09.71 E 40.92 N	DHO 23.40 kHz 07.60 E 53.08 N	TBB 26.70 kHz 27.31 E 37.40 N	GBZ 22.10 kHz 02.87 W 54.73 N	ITS 45.90 kHz 14.43 E 37.12 N
Belgrade 20.40 E 44.80 N	973 km general overview	1310 km single case study	1005 km general overview	1993 km general overview	989 km single case study
Graz 15.48 E 47.04 N	820 km general overview	875 km single case study	1445 km general overview	1541 km general overview	1105 km single case study

Case study of transmitter amplitude variations at terminator times

In this Section we consider amplitude variations around the terminators, i.e., during the transition from E- to D-layer (sunrise) and vice versa (sunset). Regular patterns are due to solar Lyman-alpha modulations connected with wave excitations where additional external influences could occur due to solar flares or internal sources via the atmosphere and the ionosphere, e.g., atmospheric gravity waves (AGWs). For the two days of the study the composite solar Lyman-alpha irradiance is 8.48732 mW/m^2 (3. May 2024, 12 UTC) and with 9.99519 mW/m^2 higher for the 5. Aug 2024, 12 UTC (these data were accessed via the LASP Interactive Solar Irradiance Data center, LISIRD).

a) Case study of DHO VLF transmitter signal with medium solar flare activity (3. May 2024)

The top panel of Figure 2 shows the amplitude variations recorded on 3. May 2024 during a medium solar flare activity. Sunrise and sunset data (civil time) are indicated by a vertical red color line for Belgrade and black one for Graz. We find that both DHO signals exhibit similar fluctuations during the day observation. However, a difference of intensity level of about 10 dB is found when combining Graz and Belgrade observations as clearly seen in Figure 2. The time resolution for Belgrade observations is one minute (red line in top panel of Figure 2), and for Graz is one second (blue line in top panel of Figure 2) and one minute (green line in top panel of Figure 2). It is important to note that Belgrade data have been slightly adjusted (offsets) to enable visual comparison.

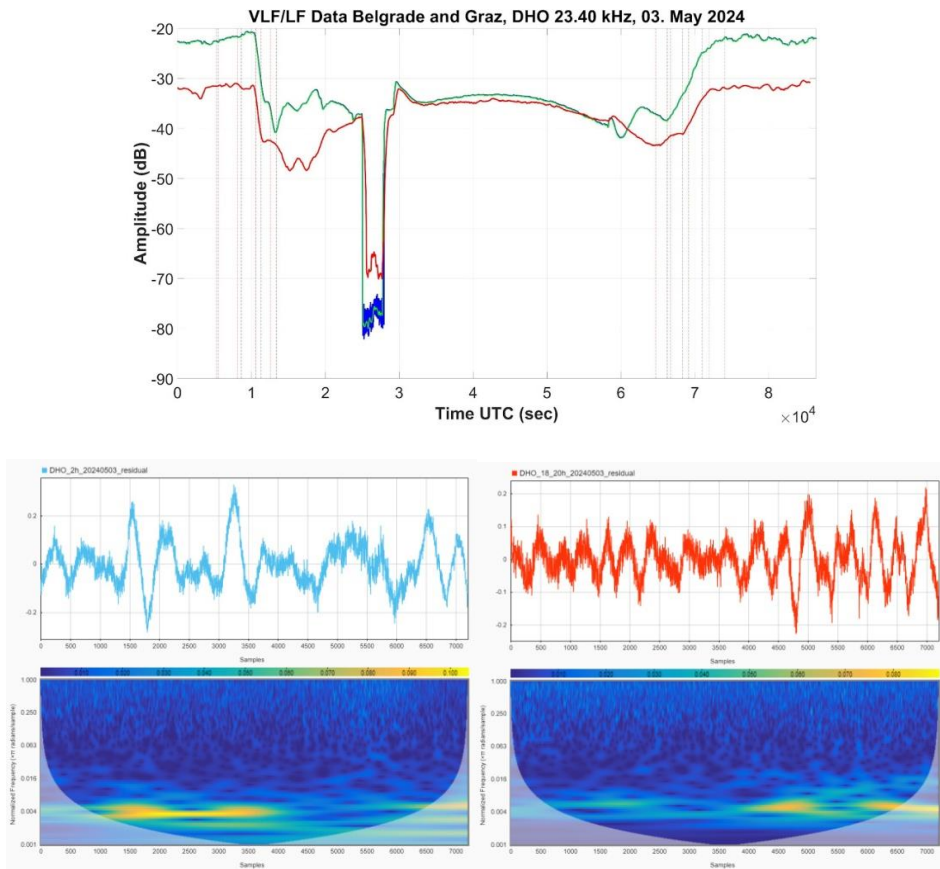


Fig. 2. Top panel: VLF DHO 23.40 kHz transmitter amplitude signal recorded on 3. May 2024, at Belgrade (red line) and Graz (blue line) reception stations. The bottom panels display the residual (bottom above panels) and the wavelet spectrum (bottom below panels).

The residuals shown in the bottom upper panels of Figure 2 are the difference between the DHO measured amplitude signal and the smoothed DHO amplitude using Savitzky-Golay filter. Those residuals are considered two hours before and after sunrise (bottom upper left panel of Figure 2) and sunset (bottom upper right panel of Figure 2) terminators. We find clear minima at terminators related to the ionospheric layers, i.e., D- and E-layers. Those residual minima appear when considering the wavelet spectrum of DHO signal as displayed in the bottom lower left panel for the sunrise and in the bottom lower right panel for the sunset terminators. We note the presence of wave activities with periods of about 500 seconds occurring at terminator times.

b) Case study of ITS VLF transmitter signal with high solar flare activity (5. August 2024)

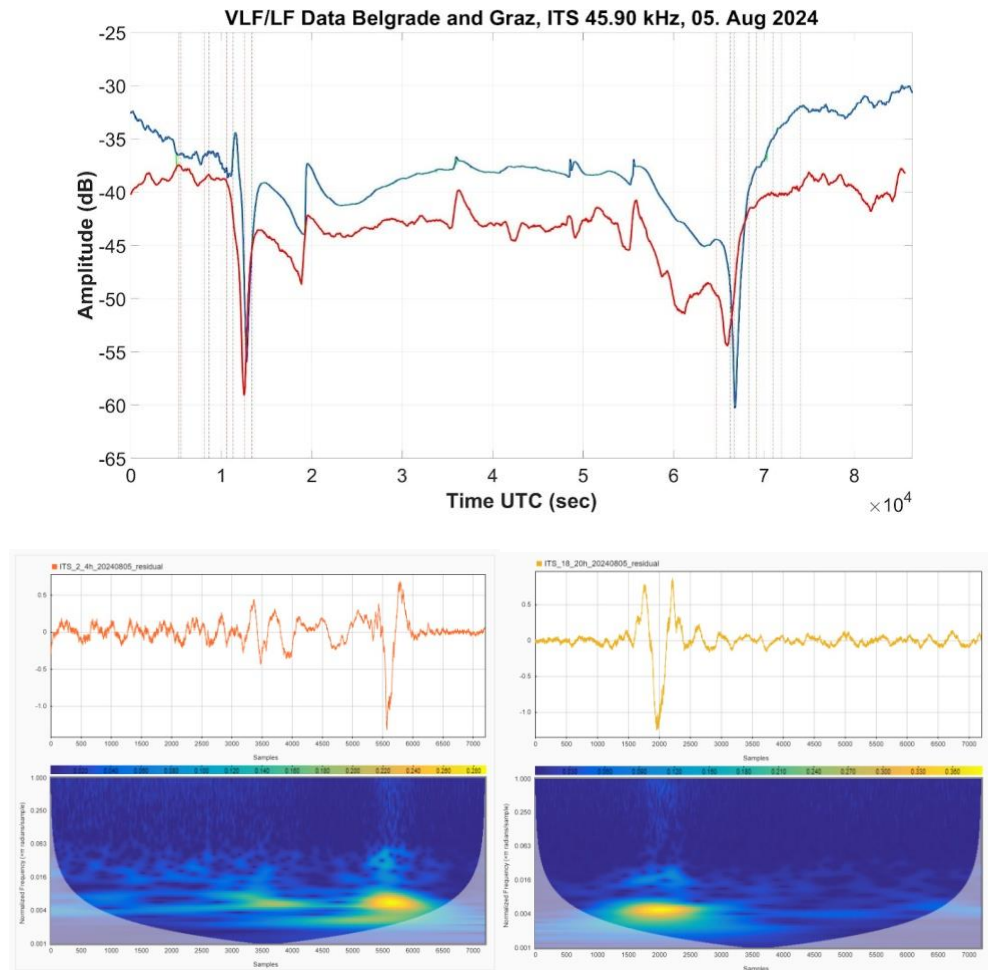


Fig. 3. Top panel: Top panel: VLF ITS 45.90 kHz transmitter amplitude signal recorded on 5. August 2024, at Belgrade (red line) and Graz (blue line) reception stations. The bottom panels display the residual (bottom upper panels) and the wavelet spectrum (bottom lower panels).

The top panel of Figure 3 displays the amplitude variations of ITS transmitter signal recorded on 5. August 2024 during a high solar flare activity. Vertical red and black color lines indicate, respectively, the sunrise and sunset terminators for Belgrade and for Graz. Like in the case of the event of 3. May 2024 the Belgrade data have been slightly adjusted (offsets) to enable visual comparison. Also, the

time resolutions used for the data processing of Belgrade and Graz observations are similar to those considered in Figure 2. Generally, ITS amplitude variations at Belgrade and Graz are found similar but exhibit a difference of 10 dB during the day and the night observations. The high solar activity is due to two X-class solar flares, accompanied by several M-class flares, recorded by GOES satellite in the wavelength range 0.1-0.8 nm. The first X-class flare occurs at about 13:40 UT (49200 sec) with a flux equal to $1.73 \cdot 10^{-4} \text{ W/m}^2$, and the second one happens at about 15:20 UT (55200 sec) with a flux equal to $1.17 \cdot 10^{-4} \text{ W/m}^2$.

The residuals shown in the bottom upper panel of Figure 3 are also considered two hours before and after sunrise (bottom upper left panel of Figure 3) and sunset (bottom upper right panel of Figure 3) terminators. We see clearly a pronounced and important minima at terminators when compared to the previous event (i.e., 3. May 2024). The increase of the residual minima is directly related to the solar flare effects on the ionospheric layers particularly at terminators. The wavelet spectrum of ITS signals show similar fluctuation as displayed in the bottom lower left panel of Figure 3 for the sunrise and in the bottom lower right panel of Figure 3 for the sunset terminators. In this case we note the existence of wave activities with periods of about 500 seconds occurring at terminator times, and also minor ones with periods in the order of 125 second.

Conclusions

The electric field amplitude data from the two receivers coincide very well and show the benefit of combined investigations of same VLF/LF links at different sites. During the terminator times wave activities with periods of ~500 sec could be measured, additional excitations occur for the more disturbed day 5. August 2024. In general, a high sample rate enables the detection of different types of variations and characterisation of noise parameters in the Earth-ionosphere waveguide.








Acknowledgments: The authors acknowledge the support provided by the Austrian Federal Ministry of Education, Science and Research (BMBWF) (project no. RS 22/2024), and the Ministry of Science, Technological Development and Innovation of the Republic of Serbia (project 337-00-216/2023-05/188). The authors acknowledge funding provided by the Institute of Physics Belgrade through the grant by the Ministry of Science, Technological Development and Innovation of the Republic of Serbia.

References

Friedrich, M., Pock, C., Torkar, K., 2018, *J. Geophys. Res.- Space Phys.*, 123, 6737.

- Galopeau, P. H. M., Maxworth, A., Boudjada, M.Y., Eichelberger, H. U., et al., 2023, *Geosci. Instrum. Method. Data Syst.*, 12, 231.
- Mironova, I. A., Aplin, K. L., Arnold, F. Bazilevskaya, G. A., et al., 2015, *Space. Sci. Rev.*, 194, 1.
- Nina, A., 2024, *Remote Sens.*, 16, 1330.
- Nina, A., Nico, G., Mitrović, S. T., Čadež, V. M., et al., 2021, *Remote Sensing*, 13, 3, 483.
- Wait, J.R. and Spies, K.P., Characteristics of the earth-ionosphere waveguide for VLF radio waves, NBS, technical note 300, p. 96, 1964.

Specific changes in VLF signals induced by astrophysical and geophysical phenomena: possibility of applying machine learning in statistical analyses

Nina, A.,¹  Butka, P.,²  Kolarski, A.,¹  Srećković, V.A.,¹ 
Sarnovský, M.,²  Bednár, P.,²  and Popović, L.Č.³ 

¹*Institute of Physics Belgrade, University of Belgrade, Pregrevica 118, 11080 Belgrade, Serbia*

²*Technical University of Košice, Faculty of Electrical Engineering and Informatics, Department of Cybernetics and Artificial Intelligence, Letná 1/9, 042 00 Košice, Slovakia*

³*Astronomical Observatory, Volgina 7, 11060 Belgrade, Serbia*
E-mail: sandrast@ipb.ac.rs

Abstract

In this paper, we present examples of changes in VLF signals used to monitor the lower ionosphere. The mentioned changes in signal characteristics are caused by astro- and geo-phenomena. We indicate the possibility of applying machine learning in statistical analysis of these changes, which is the basis of the work on the Serbian Slovak bilateral project Detection of astrophysical and geophysical phenomena from VLF radio measurements using machine learning methods.

Introduction

Spatio-temporal variations in the Earth's ionosphere are the result of the influence of numerous phenomena in space and different areas of our planet. Changes in ionospheric parameters, and, consequently, signal parameters used for its monitoring, can be specific characteristics for one phenomenon. These specificities enable the detection of phenomena indirectly, based on analyses of ionospheric disturbances and relevant electromagnetic signals, among which are very low frequency (VLF) radio signals.

Statistical analysis of changes in certain characteristics requires the application of machine learning, especially neural networks/deep learning methods. It represents one of the examples of the necessity of cooperation of scientists in different specific fields with scientists in the field of data science. One such collaboration related to the monitoring of the low ionosphere with VLF signals was

established between scientists from the Institute of Physics Belgrade, University of Belgrade and the Astronomical Observatory in Belgrade, Serbia and the Technical University of Košice (Faculty of Electrical Engineering and Informatics, Department of Cybernetics and Artificial Intelligence) in Košice, Slovakia. This cooperation is implemented within the Serbian Slovak bilateral project Detection of astrophysical and geophysical phenomena from VLF radio measurements using machine learning methods.

In this paper, we present the phenomena that give specific changes in VLF signals that meet the conditions to be analysed in this project. We will pay special attention to the changes in the intensity of the solar hydrogen Ly α line radiation that arrives in the observed part of the ionospheric D-region (extends in the domain of heights from 50 km to 90 km above the Earth's surface) and sudden emissions of X-radiation during solar X-ray flares.

Observations

In this paper, we present characteristic changes in the amplitude of NAA signal emitted in Cutler (USA) and recorded in Belgrade (Serbia) caused by variations in incoming Ly α radiation to the ionospheric D-region during 16 February 2011 when 15 flares were recorded by the GOES-15 satellite (see Table 1).

Table 1. The times of begins (t_{begin}), flux maxima (t_{max}), and ends (t_{end}) of solar X-ray flares recorded by the GOES-15 satellite on 16 February 2011.

No	t_{begin} (UT)	t_{max} (UT)	t_{end} (UT)	Class
1	00:58	01:05	01:10	C2.0
2	01:32	01:39	01:46	M1.0
3	01:56	02:00	02:05	C2.2
4	05:40	05:45	05:55	C5.9
5	06:18	06:22	06:29	C2.2
6	07:35	07:44	07:55	M1.1
7	09:02	09:11	09:19	C9.9
8	10:25	10:32	10:39	C3.2
9	11:58	12:02	12:05	C1.0
10	14:19	14:25	14:29	M1.6
11	15:27	15:32	15:37	C7.7
12	19:29	19:36	19:43	C1.3
13	20:11	20:15	20:19	C1.1
14	21:06	21:11	21:14	C4.2
15	23:02	00:25	01:07	C2.8

Phenomena that cause specific changes

These phenomena can be divided according to the place of their origin into astro- and geo-phenomena. The most significant influence from the first group is solar radiation, while changes in the atmosphere and lithosphere belong to the second group.

- Astro-phenomena: changes in the arrival of the radiation intensity of the hydrogen Ly α line due to the rotation and revolution of the Earth and solar cycle (Gupta, 1998; Correia et al. (2011); Thomson & Clilverd, 2000, Nina et al. 2021), solar X-ray flare (Nina 2022), solar eclipse (Ilić et al., 2017), gamma ray bursts (Inan et al., 2007, Nina et al., 2015).
- Geo-phenomena: lightning (Inan et al. 2010), lightning induced electron precipitation (Kolarski et al., 2022).

In addition to these cases for which previous studies have clearly confirmed the connection of phenomena with relevant changes, there are also changes for which the considered connections are still being determined. Among them are mentions in the characteristics of VLF signals before earthquakes (Biagi et al., 2011; Nina 2024) and tropical cyclones (Nina et al., 2017).

Results

In this paper, we present characteristic changes in the amplitude of NAA signal emitted in Cutler (USA) and recorded in Belgrade (Serbia) caused by variations in incoming Ly α radiation to the ionospheric D-region during 16 February 2011 when 15 flares were recorded by the GOES-15 satellite.

The daily variations of the X-ray flux recorded by the GOES-15 satellite, and the considered signal are shown in Fig. 2 (upper and bottom panels, respectively). The propagation path of this signal can be completely during the daytime (white area) or nighttime (gray areas) period, but also partially in sunlit side (during the transition from night to day and day to night; hatched areas).

Typical changes in signal amplitude during the day and under the influence of increased solar K radiation can be seen in Fig. 2. These regularities, on the basis of which further statistical studies can be carried out using machine learning, can be described as follows:

- The signal has the highest amplitude values when the path is completely nocturnal,
- The beginning of the decrease of the amplitude indicates the beginning of the insolation of the observed signal path. During the period of partial insolation of the path, the amplitude of the signal varies with pronounced minima.
- During a fully sunlit path, the amplitude first tends to increase and then decrease.

- The beginning of amplitude value variations indicates the beginning of the period of partial sunshine of the path, which ends by reaching higher values typical for the night path of the observed signal.

These changes are visible throughout the year, but the duration of the marked periods as well as the amplitude values change (Nina et al., 2017).

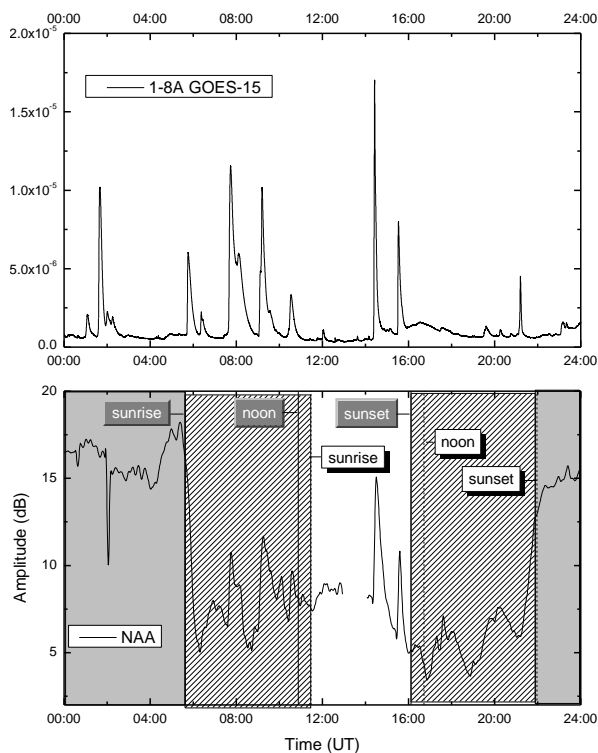


Fig. 2. Upper panel: X-ray flux recorded by the GOES-15 satellite. Bottom panel: VLF signal emitted by NAA transmitter located in the USA, and registered in Belgrade by AbsPAL receiver on 16 February 2011.

A comparison of the displayed panels shows that the amplitude of the signal changes due to the influence of the radiation emitted by solar X-ray flares during the daytime and partially sunlit path. These changes occur a few tens of seconds after the start of the increase in X radiation on the satellite and their characteristics can also be analysed using machine learning in statistical analyses.

For the machine learning part, we will follow the methodology known as CRISP-DM - Cross-industry standard process for data mining (Wirth et al., 2000). This methodology consists of problem and data understanding, data preparation, modelling (phase where machine learning models are created), and validation phases.

The machine learning project has four phases:

- **Problem identification and analysis** – this phase focused on analysis of interesting types of events (astrophysical and geophysical phenomena) for detection based on machine learning. Selected events were described in previous sections of this paper.
- **Data preparation** – in this phase, which is currently running, we focus on preparation of datasets for the machine learning process. Identified phenomena for detection were analysed in detail for ML purposes. The main aim is to prepare training, validation and testing datasets for the machine learning modelling step. It also includes selection of types of models, any data augmentation techniques, annotation of part of data, etc.
- **Building of machine learning models** – during this phase we will focus on the modelling step, i.e., creation and validation of machine learning models based on datasets prepared in the previous phase.
- **Evaluation of machine learning models** – during this step, created models will be more deeply analysed according to their effectiveness in detection of selected phenomena.

The main candidates for family of machine learning models, which we will analyze, design and test during the third phase, will be methods used for analysis of time series based on neural networks techniques, mainly from the area of deep learning models (Goodfellow et al., 2016), especially for models oriented on time series forecasting (Benidis et. al. 2023). Most popular methods in this area include recurrent deep learning architectures (Salem 2022), e.g., LSTM (Long Short-Term Memory), Conv1D (Convolution 1D neural network), and transformer-based architectures, or their different combinations (hybrid architectures). The design of architectures of models will also follow simple adaptation methodology, from analysis of data and preparation of sampling for training datasets when necessary (e.g., over-sampling, under-sampling, augmentations, etc.), preparation of evaluation criteria, selection of starting architectures (usually re-use of existing ones), their adaptation and optimization, training and testing of final models.

From a technological point of view, cloud-based environment called DATALAB (managed by the Technical University in Kosice, Slovakia) will be used for all data processing. It provides a web-based Jupyter Lab interface and processing power with several hundreds of CPUs, GPU-cards for effective training, and data storage (NAS), all used preferably with python, sci-kit, tensorflow/keras, pytorch, and many other packages used for data analysis and machine learning.

Summary

In this paper, the possibility of applying machine learning in statistical analyses of changes in VLF signals caused by various astro- and geo-phenomena is pointed out. This possibility is based on the specific characteristics of the mentioned




changes. In this study, the changes occurred on 16 February 2011 are shown as examples that meet the conditions to be analysed in the Serbian Slovak bilateral project Detection of astrophysical and geophysical phenomena from VLF radio measurements using machine learning methods.

Acknowledgments: The authors acknowledge the support provided by the Slovak APVV agency (project SK-SRB-23-0029), and the Ministry of Science, Technological Development and Innovation of the Republic of Serbia (project 337-00-3/2024-05/11). The authors acknowledge funding provided by the Institute of Physics Belgrade and the Astronomical Observatory (the contract 451-03-68/2020-14/200002) through the grants by the Ministry of Science, Technological Development and Innovation of the Republic of Serbia.

References

- Arnaud, F., Kolarski, A., Srećković, V.A., Mijić, Z., 2023, *Universe*, 9, 474.
- Benidis, K., et al., 2023, *ACM Comput. Surv.*, 55, 6, art. no. 121.
- Biagi, P.F., Maggipinto, T., Righetti, F., Loiacono, D., Schiavulli, L., et al. 2011, *Nat. Hazards Earth Syst. Sci.* 11, 333–341.
- Goodfellow, I., Bengio, Y., Courville, A, 2016, *Deep learning*, MIT Press.
- Gupta, S., 1998, *Adv. Space Res.*, 21(6), 875-881.
- Ilić L., Kuzmanoski M., Kolarž P., Nina A., et al., 2018, *J. Atmos. Solar-Terr. Phys.* 171, 250-259.
- Inan U.S., Lehtinen N.G., Moore R.C., Hurley K., et al. 2007, *Geophys. Res. Lett.* 34, L08103.
- Inan U.S., Cummer S.A., Marshall R.A., 2010, *J. Geophys. Res.-Space* 115, A00E36.
- Kolarski, A., Srećković, V.A., Mijić, Z.R, 2022, *Appl. Sci.* 12, 582.
- Nina A., Simić S., Srećković V.A., Popović L.Č., 2015, *Geophys. Res. Lett.* 42, 8250.
- Nina, A., Radovanović, M., Milovanović, B., Kovačević, et al., 2017, *Adv. Space Res.* 60(8), 1866-1877.
- Nina, A., Nico, G., Mitrović, S.T., Čadež, V.M., Milošević, I.R. et al., 2021, *Remote Sens.* 13, 483.
- Nina, A., 2024, *Remote Sens.* 2024, 16, 397.
- Salem, F.M., 2022, *Recurrent Neural Networks*, Springer International Publishing.
- Thomson, N. R, Clilverd, M. A., 2000, *J. Atmos. Solar-Terr. Phys.* 62 (7), 601-608.
- Wirth, R., Hipp, J., 2000, CRISP-DM: Towards a standard process model for data mining. In: *Proceedings of the 4th international conference on the practical applications of knowledge discovery and data mining*, 2000, Vol. 1, 29-39.

Investigating Collisional and Radiative Processes: Important Datasets for Molecular Dynamics

Srećković, V.A.,¹  Iacob, F.²  and Vujčić, V.³ 

¹*Institute of Physics Belgrade, University of Belgrade, Pregrevica 118, Belgrade, Republic of Serbia*

²*West University of Timișoara, Vasile Părvan Boulevard, 300233, Romania*

³*Astronomical Observatory, Volgina 7, 11060 Belgrade 38, Serbia
E-mail: vlada@ipb.ac.rs*

According to García & Fuss (2012) and Verkhovtsev et al. (2016), understanding complex processes induced by photons and particles is a significant challenge in today's world. These processes could, for example, result in energy conversion and storage or be critical to the creation of novel light sources (Mason et al. 2014). In recent decades, new experimental techniques and computational chemistry methods have emerged as important tools for studying molecular interactions and dynamics. Furthermore, one can note the present importance of investigating collisional and radiative processes, as well as the associated A&M data (VAMDC, RADAM) (see, for example, Dubernet et al. 2016). Today, the scientific community and industry require access to such molecular data (Marinković et al. 2017). The purpose of this work is to investigate collisional and radiative processes of small molecules and give data for characterization and chemistry of such systems. We will present, discuss, compare, and analyze cross sections and rate coefficients. The results, i.e. the created datasets/databases, can be used for important activities such as modeling, industry, synchrotron experiments, and so on (Giuliani et al. 2014; Milosavljevic et al. 2011).

Acknowledgments: This work was funded by the Institute of Physics Belgrade, University of Belgrade, through a grant by the Ministry of Science, Technological Development, and Innovations of the Republic of Serbia. We acknowledge the support the Science Fund of the Republic Serbia, Grant No. 3108/2021—NOVA2LIBS4fusion and COST Action CA20129 "Multiscale Irradiation and Chemistry Driven Processes and Related Technologies" (MultiChem).

References

- Dubernet, M. L., Boudon, V., Culhane, J. L., Dimitrijević, M. S., Fazliev, A. Z., Joblin, C., ... & Zeippen, C. J. (2010). Virtual atomic and molecular data centre. *Journal of Quantitative Spectroscopy and Radiative Transfer*, 111(15), 2151-2159.
- García G., Fuss M.C. (eds.), *Radiation Damage in Biomolecular Systems* (Springer, 2012)
- Giuliani, A., Milosavljević, A. R., Canon, F., & Nahon, L. (2014). Contribution of synchrotron radiation to photoactivation studies of biomolecular ions in the gas phase. *Mass Spectrometry Reviews*, 33(6), 424-441.
- Marinković, B. P., Jevremović, D., Srećković, V. A., Vujčić, V., Ignjatović, L. M., Dimitrijević, M. S., & Mason, N. J. (2017). BEAMDB and MolD—databases for atomic and molecular collisional and radiative processes: Belgrade nodes of VAMDC. *The European Physical Journal D*, 71, 1-9.
- Mason, N. J., Nair, B., Jheeta, S., & Szymańska, E. (2014). Electron induced chemistry: a new frontier in astrochemistry. *Faraday Discussions*, 168, 235-247.
- Milosavljević, A. R., Nicolas, C., Lemaire, J., Dehon, C., Thissen, R., Bizau, J. M., ... & Giuliani, A. (2011). Photoionization of a protein isolated in vacuo. *Physical Chemistry Chemical Physics*, 13(34), 15432-15436.
- Verkhovtsev, A., Surdutovich, E., & Solov'yov, A. V. (2016). Multiscale approach predictions for biological outcomes in ion-beam cancer therapy. *Scientific reports*, 6(1), 27654.

New molecular dataset for planet formation chemistry and modeling

Srećković, V.A.,¹  Pop, N.,²  Vujčić, V.,³  Dimitrijević, M.S.,³ 
Christova, M.D.⁴  and Mijić, Z.¹ 

¹*Institute of Physics Belgrade, University of Belgrade, Pregrevica 118, Belgrade, Republic of Serbia*

²*Politehnica University of Timisoara, Timisoara, Romania*

³*Astronomical Observatory, Volgina 7, 11060 Belgrade 38, Serbia*

⁴*Department of Applied Physics, TU Sofia, Bulgaria*

E-mail: vlada@ipb.ac.rs

Detailed astrochemical models are essential for interpreting observations of interstellar and circumstellar molecules because they allow important physical features of the gas and its evolutionary history to be derived (Williams and Cieza 2011). Advances in astrochemical models are linked to changes in astrochemical databases, as well as experimental and theoretical estimations of rate coefficients (see e.g. Öberg et al. 2021). The science community now need access to such molecular data, including preferred ones, for further modeling, and it is critical to our knowledge of the chemistry of planet formation. As a result, atomic and molecular datasets and databases (such as VAMDC) have become critical for constructing models and simulations (see Albert et al. 2021 and references therein). The analysis of the studied rates provides valuable information on the presence of species. As a result, it is critical to investigate not only radiative processes, but also concurrent processes involving molecular ions, such as dissociative recombination (Kamp et al., 2017). Our goal is to calculate, compare, and analyze cross sections and rate coefficients for molecular ions such as hydrogen and helium for a various model parameters.

Acknowledgments: This work was funded by the Institute of Physics Belgrade, University of Belgrade, through a grant by the Ministry of Science, Technological Development, and Innovations of the Republic of Serbia. We acknowledge the support the Science Fund of the Republic Serbia, Grant No. 3108/2021—NOVA2LIBS4fusion and COST Action CA22133 - The birth of solar systems (PLANETS).

References

- Albert, D.; Antony, B.; Ba, Y.A.; Babikov, Y.L.; Bollard, P.; Boudon, V.; Delahaye, F.; Del Zanna, G.; Dimitrijević, M.S.; Drouin, B.J.; Dubernet, M.-L.; et al. A Decade with VAMDC: Results and Ambitions. *Atoms* 2020, 8, 76.
- ALMA Partnership et al., 2015, *ApJL*, 808, L3
- Kamp, I., Thi, W. F., Woitke, P., Rab, C., Bouma, S., & Menard, F. (2017). Consistent dust and gas models for protoplanetary disks-II. Chemical networks and rates. *Astronomy & Astrophysics*, 607, A41.
- Öberg, K. I., Guzmán, V. V., Walsh, C., Aikawa, Y., Bergin, E. A., Law, C. J., ... & Zhang, K. (2021). Molecules with ALMA at Planet-forming Scales (MAPS). I. Program overview and highlights. *The Astrophysical Journal Supplement Series*, 257(1), 1.
- Miyake, S., Gay, C. D., & Stancil, P. C. (2011). Rovibrationally resolved photodissociation of HeH⁺. *The Astrophysical Journal*, 735(1), 21.
- Visser, R., Bruderer, S., Cazzoletti, P., Facchini, S., Heays, A. N., & van Dishoeck, E. F. (2018). Nitrogen isotope fractionation in protoplanetary disks. *Astronomy & Astrophysics*, 615, A75.
- Walsh, C., Nomura, H., Millar, T. J., & Aikawa, Y. (2012). Chemical processes in protoplanetary disks. II. On the importance of photochemistry and X-ray ionization. *The Astrophysical Journal*, 747(2), 114.
- Williams, Jonathan P., and Lucas A. Cieza. "Protoplanetary disks and their evolution." *Annual Review of Astronomy and Astrophysics* 49 (2011): 67-117.

Earth's Lower Ionosphere under energetic events: solar flares and gamma ray bursts as drivers for VLF signal perturbations

Kolarski, A.,¹  Nina, A.,¹  Srećković, V.A.¹  Arnaut, A.¹  and Langović, M.¹ 

¹*Institute of Physics Belgrade, University of Belgrade, Pregrevica 118, 11000 Belgrade, Serbia*

E-mail: aleksandra.kolarski@ipb.ac.rs

Earth's lower ionospheric perturbations induced by different phenomena, such as energetic solar flare events of high class on one hand and gamma ray bursts on the other, were examined through a remote sensing approach by utilization of VLF radio signals (Very Low Frequency, 3-30 kHz) propagating globally within Earth-ionosphere waveguide. Solar X-ray radiation data were taken from Geostationary Operational Environmental Satellites (GOES) database, while data related to gamma ray bursts were taken from Swift satellite database. VLF data used in this research are from Belgrade database, obtained from receiver system located at the Institute of Physics in Belgrade, Serbia, cover period of several consecutive years during solar cycle 24. Based on VLF registrations from European transmitters, temporal evolution and general patterns in VLF signal perturbations related to these events were examined, with main results related to D-region plasma behavior under such energetic events presented here.

Key words: X-ray flares, gamma ray bursts, ionosphere, VLF signal perturbation

Photodissociation processes in non-symmetric systems

Tošić, S.,¹  Srećković, V.A.¹  and Vujčić, V.² 

¹*Institute of Physics Belgrade, University of Belgrade, Pregrevica 118, 11080 Belgrade, Serbia.*

²*Astronomical Observatory, 11060 Belgrade, Serbia.
E-mail: seka@ipb.ac.rs*

New findings in the fields of atmospheric science, astrochemistry etc. have been made possible by recent experimental and theoretical developments. One of the most crucial processes in planetary atmospheres and interstellar media is photodissociation. A brief overview of the fundamental physical processes including photodissociation and photoionization of molecules of astronomical interest as well as new astrophysically relevant molecular species have recently been added to the Leiden VUV cross section database (Hrodmarsson and Dishoeck, 2023). The importance of these data for analyzing observations and measurement results in a variety of fields is also growing (Vujcic et al., 2023). On the other hand, despite of involvement of both ionic and neutral alkali hydride species in a number of astrophysical and astrochemical processes (Sreckovic et al., 2021), only a small amount of theory and observation is known about their spectroscopy, especially when it comes to molecule ions. Here we present results of investigations of the mechanisms of photodissociation processes in non-symmetric systems/configurations involving ions, molecular ions, hydrogen, helium, and alkali atoms. Quantum mechanical analysis of the cross-sections and spectral rate coefficient data has been carried out.

Acknowledgments: This research was supported by the Science Fund of the Republic Serbia [Grant no. 3108/2021, NOVA2LIBS4fusion and Grant No. 7749560, EGWIn]

References

- H R Hrodmarsson and E F Dishoeck (2023). *A&A*, 675, A25.
V Vujcic *et al.* (2023) *Phys. Chem. Chem. Phys.*, 25(40), 26972.
V A Sreckovic *et al.* (2021) *Molecules*, 26(1), 151.

Machine Learning Classification Difficulties of VLF Amplitude Variations Around the Terminator

Arnaud, F.,¹  Kolarski, A.,¹  Langović, M.,¹  Srećković, V.A.¹  and Jevremović, S.² 

¹*Institute of Physics Belgrade, University of Belgrade, Pregrevica 118, Belgrade, Republic of Serbia*


²*Scientific Society Isaac Newton Belgrade, Volgina 7, Belgrade, Republic of Serbia*
E-mail: filip.arnaut@ipb.ac.rs

Previously, very low frequency (VLF) ionospheric amplitude data was employed in various machine learning (ML) classification efforts (Arnaud, Kolarski, 2023; Arnaut et al., 2023; Arnaut et al., 2024), where the problem was defined as a binary classification task, determining whether a given data point in the test dataset was anomalous (e.g., solar flare events, instrument errors, nighttime signals, outliers) or a normal daytime signal. In a multiclass classification problem, each class must be clearly defined to prevent overlap and minimize the risk of false positives and/or false negatives. The analysis for this brief communication displays that the challenges in classifying nighttime versus daytime VLF amplitude signals occur at the terminator, a transitional zone between daytime-nighttime and nighttime-daytime signals. The majority of false positives and/or false negatives occur in this zone. Possible strategies for enhancing predictive power in this area may include statistical techniques such as cluster analysis or other methods that can be employed post-classification to further augment the overall efficacy of the approach.

References

- Arnaud, F. & Kolarski, A., 2023. Machine learning approach for distinguishing daytime and nighttime ionospheric conditions on VLF signals related to solar flares during 2011. In XX Serbian Astronomical Conference, 16-20 October 2023, Belgrade, Serbia. Book of Abstracts, Astronomical Observatory of Belgrade and Faculty of Mathematics, pp. 79
- Arnaud, F., Kolarski, A. and Srećković, V.A., 2023. Random forest classification and ionospheric response to solar flares: Analysis and validation. *Universe*, 9(10), p.436.
- Arnaud, F., Kolarski, A. and Srećković, V.A., 2024. Machine Learning Classification Workflow and Datasets for Ionospheric VLF Data Exclusion. *Data*, 9(1), p.17.

Electrical Breakdown in trans-1,3,3,3-Tetrafluoropropene HFO1234ze(E)

Marjanović, J.,¹  Marić, D.,¹  Dujko, S.¹  and Petrović, Z.Lj.^{2,3} 

¹*Institute of Physics, University of Belgrade, Pregrevica 118, 11080 Belgrade, Serbia*

²*Serbian Academy of Sciences and Arts, Kneza Mihaila 35, 11001 Belgrade, Serbia*

³*School of Engineering, Ulster University, Jordanstown, County Antrim BT37 0QB, United Kingdom*

E-mail: sivosj@ipb.ac.rs

Hydrofluoroolefins, unsaturated organic compounds developed as "fourth generation" refrigerants, possess only 0.1% of the Global Warming Potential (GWP) of hydrofluorocarbons (HFCs) and have negligible Ozone Depletion Potential (ODP). Their excellent eco-friendly properties make them suitable for use in air conditioning systems and they are also considered to be potential replacements for SF₆ in dielectric applications. In recent years, trans-1,3,3,3-Tetrafluoropropene (HFO1234ze(E)) has garnered the research community's interest due to its applications in medium and high voltage gas-insulated transmission and distribution equipment (HV and MV GIE), as well as in RPC particle detectors (Koch and Franck 2015, Hosl et al. 2020, Chachereau et al. 2016, Preve et al. 2017). The improvement of existing applications relies on relevant and reliable data, which can be obtained from breakdown measurements. Here, we present the results from our measurements of dc breakdown in trans-1,3,3,3-tetrafluoropropene. Our measurements are done in a centimeter-sized plan-parallel electrode system (Sivoš et al. 2020), under swarm conditions at low currents ($\sim 1 \mu\text{A}$) and low pressures ($\sim 0.05 - 3 \text{ Torr}$). In Figure 1, we present breakdown results for trans-1,3,3,3-Tetrafluoropropene (HFO1234ze(E), C₃H₂F₄) in comparison with sulfur hexafluoride (SF₆). Paschen curve of HFO1234ze(E) is recorded for electrode distance of 1 cm. The minimum breakdown voltage of 482 V occurs at $pd = 0.25 \text{ Torr cm}$ (p – pressure, d – electrode distance). The discharge ignites and operates stably at low-currents up to $\sim 0.8 \text{ Torr cm}$, but above this value discharge ignites into periodic relaxation oscillations (Kuschel et al. 2011). The breakdown voltage values for HFO1234ze (E) are slightly lower than those for SF₆ around the Paschen minimum and on the right-hand side of the Paschen curve.

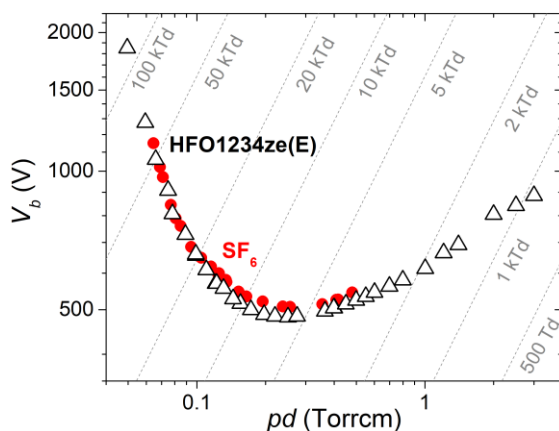


Fig. 1. Comparison of Paschen curves for trans-1,3,3,3-Tetrafluoropropene (HFO1234ze(E)) (black open triangles) and sulfur hexafluoride (SF_6) (red solid circles) (Stefanović 1998, Marić et al. 2014). Curves have been obtained for an electrode distance of 1 cm.

On the other hand, at lower pressures, the breakdown voltage of HFO1234ze(E) increases steeply and becomes nearly equal to SF_6 . Although HFO1234ze(E) shows significant insulation potential, it is not sufficient as a standalone substitute for SF_6 .

Acknowledgements: This research was supported by the Science Fund of the Republic of Serbia, Grant No. 7749560, project EGWIn. Zoran Lj. Petrović is grateful to the SASA project F155.

References

- Chachereau, A., Rabie, M. and Franck, C. M., 2016, *Plasma Sources Science and Technology*, 25, 045005
- Hosl, A., Pachin, J., Eguz, E., Chachereau, A., Franck, C.M., 2020, *IEEE Trans. Dielectr. Electr. Insul.*, 27, 322
- Koch, M. and Franck, C. M., 2015, *IEEE Transactions on Dielectrics and Electrical Insulation*, 22, 3260
- Kuschel, T., Stefanović, I., Škoro, N., Marić, D., Malović, G., Winter, J., and Petrović, Z. Lj., 2011, *IEEE Trans. Plasma Sci.*, 39 2692
- Marić, D., Savić, M., Sivoš, J., Škoro, N., Radmi-lović-Radjenović, M., Malović, G., Petrović, Z.Lj., 2014, *Eur. Phys. J. D*, 68, 155
- Preve, C., Piccoz, D. and Maladen, R., 2017, in *CIREN - Open Access Proceedings Journal*, 2017, 42
- Sivoš, J., Marić, D., Malović, G., Petrović, Z. Lj., 2020, *Eur. Phys. J. D* 74, 64
- Steanović, I., 1998, *Osobine difuznih električnih pražnjenja u gasovima na niskom pritisku u režimu niskih struja* [Doctoral dissertation, School of Electrical Engineering, University of Belgrade]

Elastic electron scattering by xenon atom and data coverage within BEAMDB

Marinković, B.P.,¹  Ivanović, S.Đ.¹ and Uskoković, N.A.¹

¹*Institute of Physics Belgrade, Pregrevica 118, 11080 Belgrade, Serbia*
E-mail: bratislav.marinkovic@ipb.ac.rs

We investigated data on elastic electron scattering by xenon atom in the intermediate electron energy range (from 10 eV to 100 eV). Our preliminary survey have been contrasted to those data curated within BEAMDB - Belgrade Electron/Atom (Molecule) DataBase. BEAMDB¹ is one of the VAMDC (Virtual Atomic and Molecular Data Centre) nodes specialized for data on electron interactions (elastic scattering, excitation, ionization, energy loss spectra, threshold spectra) with atomic species. Previous recent work on xenon atom involves Auger spectra (Jureta *et al.* 2023). We just want to mention some of the earlier work on electron scattering that includes excitations (Filipović *et al.* 1988), ionization (Stephan and Märk, 1984) and elastic scattering (Cho *et al.* 2006).

Acknowledgements: This work has been partially supported by the Science Fund of the Republic of Serbia, Grant No. 6821, Atoms and (bio)molecules-dynamics and collisional processes on short time scale – ATMOLCOL.

References

- Jozo J. Jureta, Bratislav P. Marinković, Lorenzo Avaldi, “The N_{4,5}-OO Auger and “N₃”-M_{4,5}O_{2,3} Coster-Kronig spectra of xenon induced by electron impact”, *Adv. Space Res.* **71**(2) 1338-1351 (2023). [doi: 10.1016/j.asr.2022.06.066](https://doi.org/10.1016/j.asr.2022.06.066)
- D. Filipović, B. Marinković, V. Pejčev and L. Vušković, “Electron-impact excitation of xenon at incident energies between 15 and 80 eV”, *Phys. Rev. A* **37**(2), 356-64 (1988). [doi: 10.1103/PhysRevA.37.356](https://doi.org/10.1103/PhysRevA.37.356)
- K. Stephan and T. D. Märk, “Absolute partial electron impact ionization cross sections of Xe from threshold up to 180 eV” *J. Phys. Chem.* **81**, 3116-3117 (1984). [doi: 10.1063/1.448013](https://doi.org/10.1063/1.448013)
- H Cho, R P McEachran, S J Buckman, D M Filipović, V Pejčev, B P Marinković, H Tanaka, A D Stauffer and E C Jung, “Absorption effects in intermediate energy elastic electron scattering from xenon”, *J. Phys. B: At. Mol. Opt. Phys.* **39**(18), 3781-3790 (2006). [doi:10.1088/0953-4075/39/18/008](https://doi.org/10.1088/0953-4075/39/18/008)

¹ <http://servo.aob.rs/emol/>

Fitting of the current signal of the Pulsed Townsend experiment with the gradient descent algorithm

Simonović, I.B.,¹  Bošnjaković, D.V.¹  and Dujko, S.¹ 

¹*Institute of Physics, University of Belgrade, P.O. Box 68, 11080 Belgrade, Serbia*
E-mail: sasa.dujko@ipb.ac.rs

The Pulsed Townsend experiment is used for determining the transport coefficients for a swarm of electrons in gases (see e.g., Casey 2021, De Urquijo 2007, Haefliger 2018). These transport coefficients include drift velocity, longitudinal diffusion and the effective ionization coefficient. In general, these transport coefficients are determined by fitting an analytical expression, in which the current signal is expressed in terms of these transport coefficients, to the actual current signal that is measured in the experiment by a nonlinear curve fitting procedure. In the literature, different analytical expressions for the current signal are used by different authors, and the employed nonlinear curve fitting procedures are not always publicly available. For this reason, a systematic study of the fitting of the current signal of the Pulsed Townsend experiment is long overdue, and this work makes first steps in that direction.

In this contribution, we investigate the applicability of the gradient descent algorithm for the fitting of the current signal of the Pulsed Townsend experiment. The gradient descent algorithm is a method for unconstrained mathematical optimization, that is commonly used to train machine learning models including linear regression, logistic regression, neural networks, and support vector machines (see e.g. Bishop 2006). This algorithm minimizes the desired differentiable multivariate function by making repeated steps in the direction opposite to the gradient.

In this contribution, we investigate two different analytical expressions for the current signal from the Pulsed Townsend experiment. We have defined two machine learning models that implement these expressions in the *torch.nn.Module* class from the PyTorch library. PyTorch is an open-source library for machine learning, data science, and artificial intelligence, that has been originally developed by Meta AI (see e.g. Ketkar 2021). The transport coefficients, that are determined from the current signal of the Pulsed Townsend experiment, are included in these models as trainable parameters. The models are trained by employing the *torch.optim.Adam* class, which implements the Adam variant of the gradient descent algorithm (see e.g. Barakat 2021), and by using the data that is generated from the corresponding

analytical expressions, by employing NumPy and SciPy open-source libraries (see e.g. Bressert 2013). Three different learning rates are used for drift velocity, diffusion coefficient, and the effective ionization coefficient, to optimize the convergence of the training algorithm, as these three coefficients have different orders of magnitude. We have observed that excellent convergence is obtained for all four combinations of the two PyTorch models and the two current signals. However, it is important to first estimate the initial guess for the drift velocity from the time at which the current signal is being rapidly reduced, due to the absorption of the electron swarm at the anode.

Acknowledgments: This work is supported by the Science Fund of the Republic of Serbia, Grant No. 7749560, Exploring ultra-low global warming potential gases for insulation in high-voltage technology: Experiments and modelling EGWIn.

References

- Barakat A., Bianchi P., 2021, *SIAM Journal on Optimization*. 31 244
- Bishop C. M., Nasrabadi N. M. *Pattern recognition and machine learning*. New York: Springer, 2006.
- Bressert E., *SciPy and NumPy: an overview for developers*. Gravenstain Highway North Sebastopol: O'Reilly Media, Inc, 2013
- Casey M. J., Stokes P. W., Cocks D. G., Bošnjaković D., Simonović I., Brunger M. J., Dujko S., Petrović Z. L., Robson R. E., White R. D., 2021, *Plasma Sources Sci. Technol.* 30, 035017.
- De Urquijo J., Juarez A. M., Rodríguez-Luna J. C., Ramos-Salas J. S., 2007, *IEEE transactions on plasma science*. 35, 1204.
- Haefliger P., Franck C. M., 2018, *Review of Scientific instruments*. 89, 023114.
- Ketkar N., Moolayil J., Ketkar N., Moolayil J., *Introduction to pytorch. Deep learning with python: learn best practices of deep learning models with PyTorch*. Apress, Berkeley, CA, 2021:27-91

Spatio-temporal dynamics of a microsecond pulsed glow discharge

Krstić, I.B.,¹  Obradović, B.M.¹  and Kuraica, M.M.¹ 

¹*University of Belgrade – Faculty of Physics, Belgrade, Serbia*
E-mail: obrat@ff.bg.ac.rs

As a type of pulsed discharges, microsecond pulsed glow discharges (μs -PGD) brought an improvement of the analytical characteristics of the GD sources for several optical and mass spectrometric methods. Advantages of μs -PGD are increasing signal outputs and the temporal resolution of analytical species from concomitant species in the discharge plasma. Another benefit of μs -PGD is that even though instantaneous power is higher, the average power can be significantly lower than in millisecond PGD, resulting in reduced thermal stress of the analyzing sample. The higher instantaneous power of the μs -PGD is closely related to the so-called “pre-peak”, a spike in the electrical current and a spike of plasma radiation at the leading edge of the discharge pulse. The radiation pre-peak, together with an increased radiation in afterglow for some spectral lines (after-peak) are responsible for the improvement of the analytical characteristics of the PGD in optical emission spectrometry. Here we present results of measurement of spatio-temporal distributions of several atomic spectral lines of copper in a Grimm-type μs -PGD.

To run discharge, a laboratory made pulsed voltage power supply were used, with capability to ensure up to 300 W per pulse. For a space resolved emission measurements we used optical system contained of quartz lens and 1m-Spectrometer equipped with ICCD camera. Following the suggestion (Alberts et al, 2010) measurements have done by using the frequency of 5 kHz and the pulse width of 30 μs . 170 μs off-time allows to investigate near afterglow of the discharge.

At the line intensity distribution, three characteristic phases (or the discharge regimes) can be resolved: the pre-peak (0 – 5 μs) caused by fast increase of the applied voltage; steady-state (5 – 30 μs) during it the voltage has a constant value, and the afterglow when the voltage is switched off, see Fig. 1. There are the two space regions, characteristic for the discharge: the CF which border is marked as L, and the NG beyond the CF region.

The distributions of Cu I 510.55 nm (4s – 4p, 1.39 – 3.82 eV) and Cu I 515.32 nm (4p – 4d, 3.79 – 6.19 eV) lines, as example for the two typical representative copper lines are presented at Fig. 1. The distributions of Cu I 510.55 nm line clearly shows the manifestation of three characteristic phase of the μs -PGD operation: pre-peak, steady-state and afterglow. In the pre-peak phase, at the

moment of the V_{\max} , line intensity distribution has a strong broad maximum positioned at 2.7 mm from the cathode. During the pre-peak phase almost entire line emission comes from the NG region. The Cu I line intensity depends on the sputtered copper atoms and as well as on the EEDF. According to the Monte Carlo analysis made for the discharge similar to ours, during the first several microseconds after the discharge is ignited, the EEDFs in the NG are characterized by a high peak corresponding to a few eV (Martín et al., 2008). Electron energy of several eV is sufficient for excitation of many copper atom's low energy levels, so intensity of such Cu I lines in the pre-peak phase can be much higher in the NG than in the CF region, even the copper atoms density is much lower in the first one.

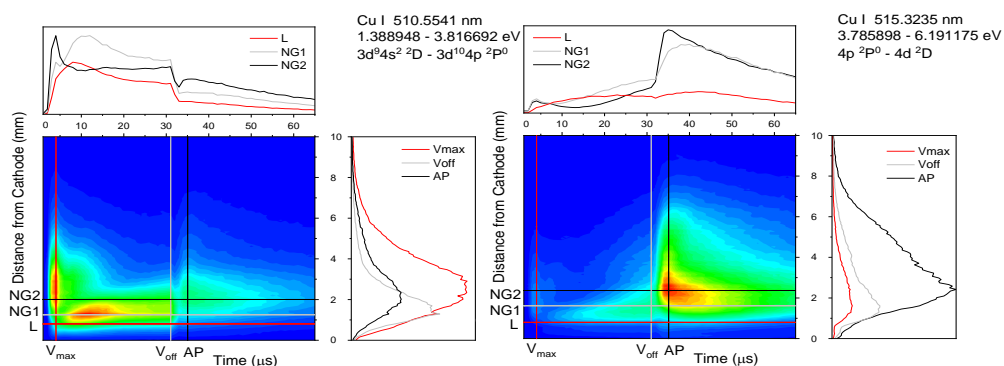


Fig. 2. Spatio-temporal distribution of Cu I lines intensities.

The observed maximum of the line intensity during the time development appears as the consequence of several simultaneous processes that influence on copper atom number: sputtering, redeposition and Penning ionization of the copper atoms. Analyzing Fig. 1 one can see that the Cu I 515.32 nm line intensity is much higher during the afterglow than during the pulse phase of the discharge. As the self-absorption is excluded for this line, increasing of the line intensity with time is evidence of increasing of the copper atom number during the steady-state phase. During the afterglow phase the line intensity greatly increases at the distances that belongs to the NG region; farther from the cathode, the increasing is higher.

Acknowledgments: This work was supported by the Ministry of Education and Science of the Republic of Serbia (Contract Number 451-03-68/2022-14/200162) and by the Science Fund of the Republic of Serbia through the Project ATTOPLASMAS # 7750277.

References

- Alberts D. et al, 2010, Spectrochim. Acta - Part B 65, 533–541.
 Martín A. et al, 2008, Spectrochim. Acta - Part B, 63 1274–1282.

Helium plasma jet as a probe for the laser irradiance measurements

Sretenović, G.B.,¹  Kovačević, V.V.,¹  Obradović, B.M.,¹ 
Kuraica, M.M.¹  and Ranitović, P.¹ 

¹University of Belgrade – Faculty of Physics, Belgrade, Serbia
E-mail: sretenovic@ff.bg.ac.rs

The knowledge of the effective value of the laser power density in the arbitrary position is usually of importance for any experimental work. It has been shown that the non-resonant laser irradiation induces line shift through the dynamical Stark effect of the excited atoms (Dubreuil et al. 1978). The effect is shown to be of order of $4 \cdot 10^{-3}$ nm/(MW·cm²) for particular helium atom transition 43S - 23P at 471.3 nm. The work included theoretical calculations based on the second order perturbation theory and the experimental confirmation utilized by continuous wave CO₂ laser irradiation of low-pressure discharge in helium.

In this work we present preliminary results of the measurements of the helium line shift caused by helium atmospheric pressure plasma jet irradiation by tunable energy (4 mJ maximum) femtosecond ytterbium doped fiber laser at 1030 nm (Pharos, Light Conversion). Atmospheric pressure plasma jets represent controllable plasma devices of simple construction that found broad applications in various fields, from material science to medicine. These devices emit spatially and temporally stabilized low electron density streamers through the helium gas stream that flows into the air (Lu et al. 2014). Thus, their construction enables generation of plasma in free space which candidates them as ideal plasma probes.

Helium atmospheric plasma jet based on the asymmetric dielectric barrier discharge was powered by 2.5 kV sinusoidal voltage at 30 kHz. The laser operated at the same frequency and its average power could be changed in range 0-20 W. The laser and the plasma jet were synchronized by means of delay generator in a manner that the laser light and the streamer appear at the same time at the same place. 1-m focal length spectrometer equipped with iCCD recorded helium emission at the particular wavelength. The laser intensity was kept below breakdown value. The recorded line profile and the line shift dependence on the applied power are given in Figure 1(a) and 1(b).

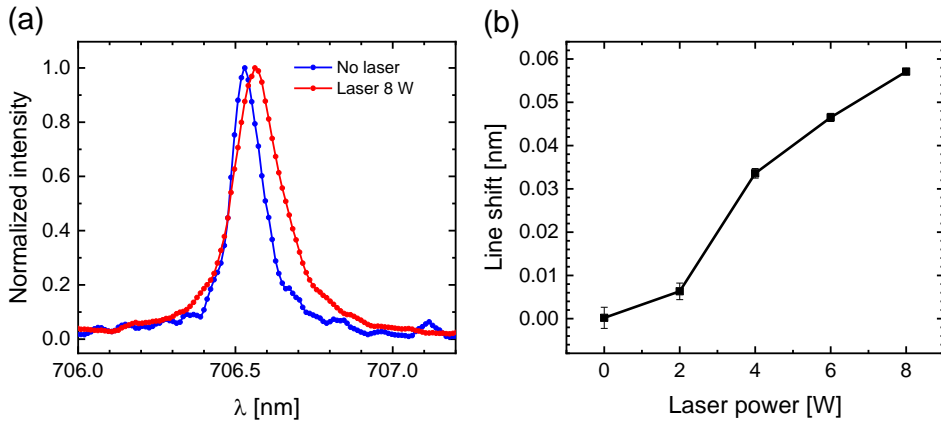


Fig. 1. (a) The examples of unshifted and shifted lines. (b) Line shift in dependence of laser power.

The preliminary results confirm the effect of the line shift induced by laser radiation. Further measurements should valorize these results and find the atomic emission line which is the best candidate for the use for the laser power density measurements.

This work was supported by the Ministry of Education and Science of the Republic of Serbia (Contract Number 451-03-68/2022-14/200162) and by the Science Fund of the Republic of Serbia through the Project ATTOPLASMAS # 7750277.

References

- Dubreuil B., Chapelle J., 1978, *Physica B+C* 94(2), 233-250.
Lu X., Naidis G. V., Laroussi M., Ostrikov K., 2014, *Phys. Rep.* 540, 123

Dissociative electron attachment to isoflurane molecule in the gas phase

Maljković, J.B.,¹  Marinković, B.P.¹  and Kopyra, J.² 

¹*Institute of Physics Belgrade, University of Belgrade, Pregrevica 118, 11080 Belgrade, Serbia*

²*Faculty of Sciences, Siedlce University, 3 Maja 54, 08-110 Siedlce, Poland*
E-mail: jelenam@ipb.ac.rs




Common halogenated anesthetic gases include halothane, isoflurane, sevoflurane, and desflurane. These gases can have varying global warming potential (GWP) and environmental effects (Langbein et al 1999). Halogenated aneastics also contribute to greenhouse gas emissions, although their impact varies based on their global warming potential GWP. We studied DEA to gas phase target by means of a crossed electron-molecular beam technique (Kopyra et al 2017). Dissociative electron attachment processes were investigated utilizing the crossed beam apparatus. In this technique the incident electron beam orthogonally intersects with molecular beam resulting in the formation of fragment anions. The calibration of the energy scale is achieved by measuring SF₆ signal, with intense resonance near 0 eV. Base pressure was in the range of $\sim 10^{-8}$ mbars and the working pressure around 3.2×10^{-7} mbars. We have measured halogenated aneathetic isofluran which showed a rich fragmentation. We have observed the following fragments: F⁻ = 19 a.m.u, Cl⁻ = 35 a.m.u, FHF⁻ = 39 a.m.u, CF₃⁻ = 69 a.m.u., C₂F₃⁻ = 81 a.m.u, C₂F₃Cl⁻ = 116 a.m.u

Acknowledgements: This work has been partially supported by the Science Fund of the Republic of Serbia, Grant No. 6821, Atoms and (bio)molecules-dynamics and collisional processes on short time scale – ATMOLCOL. The article is based upon work from COST Action CA20129 (MultiChem),

References

- Langbein T., Sonntag H, Trapp D, Hoffmann A, Malms W, Röth E P, Mörs V, Zellner R 1999, *J. Anaesth*, 82, 66
Kopyra J, Maciejewska P and Maljković J., 2017. *Beilstein J. Nanotechnol*, 8, 2257

Constraining the Deser-Woodard non-local gravity by Fundamental plane of elliptical galaxies

Borka Jovanović, V.,¹  Borka, D.,¹  Capozziello, S.^{2,3,4} and
Jovanović, P.⁵ 

¹*Department of Theoretical Physics and Condensed Matter Physics (020), Vinča
Institute of Nuclear Sciences - National Institute of the Republic of Serbia,
University of Belgrade, P.O. Box 522, 11001 Belgrade, Serbia*

²*Scuola Superiore Meridionale, Largo San Marcellino 10, 80138 Napoli, Italy*

³*Istituto Nazionale di Fisica Nucleare, Sez. di Napoli, Via Cinthia 21, 80126
Napoli, Italy*

⁴*Dipartimento di Fisica "E. Pancini", Università di Napoli "Federico II", Via
Cinthia 21, 80126 Napoli, Italy*

⁵*Astronomical Observatory, Volgina 7, P.O. Box 74, 11060 Belgrade, Serbia
E-mail: vborka@vinca.rs*

Among extended theories of gravity, there are the non-local theories of gravity. In the case when the non-local terms of such a theory are canceled out, the limit of General Relativity is obtained. Non-locality in the present context applies to field theory, and non-local field theory extends classical field theory. Here, we take non-local gravity model given in Deser & Woodard 2007.

On the other hand, the Fundamental plane (FP) is an empirical relation among three global parameters of elliptical galaxies expressed as a relationship between the central projected velocity dispersion, the effective radius, and the mean effective surface brightness within effective radius (for more details see e.g. Dressler et al. 1987, Borka Jovanović et al. 2016, Capozziello et al. 2020).

In this contribution we use freely available observations of elliptical galaxies from Burstein et al. (1997) (their effective radii, effective luminosities and characteristic velocities) in order to study if Deser-Woodard non-local gravity can recover FP of elliptical galaxies. We also use these data to constrain parameters of this gravity model and demonstrate that FP can be successfully recovered without need for dark matter hypothesis.

References

Borka Jovanović, V., Capozziello, S., Jovanović, P., Borka, D., 2016, Phys. Dark Univ., 14, 73

- Burstein, D., Bender, R., Faber, S., Nolthenius, R., 1997, *Astron. J.*, 114, 1365
Capozziello, S., Borka Jovanović, V., Borka, D., Jovanović, P., 2020, *Phys. Dark Univ.*, 29, 100573
Deser, S., Woodard, R. P., 2007, *Phys. Rev. Lett.*, 99, 111301
Dressler, A., Lynden-Bell, D., Burstein, D., Davies, R. L., Faber, S. M., Terlevich, R., Wegner, G., 1987, *Astrophys. J.*, 313, 42

Impact of Coulomb correction on the nonadiabatic tunnel ionization in an elliptically polarized laser field

Petrović, V.M.,¹  Delibašić Marković, H.S.¹  and Petrović, I.D.²

¹*Faculty of Science, University of Kragujevac, Radoja Domanovića 12, 34000 Kragujevac, Serbia*

²*Department in Kragujevac, Academy of Professional Studies Šumadija, Kosovska 8, Kragujevac, Serbia*

E-mail: violeta.petrovic@pmf.kg.ac.rs

Using a time-imaginary method rooted in the Landau-Dykhne model (Landau 1977) within the frame of the trajectory-based semiclassical approach, we developed an analytical model that investigates the impact of the Coulomb interaction between the atomic core and the escaping electron for a monochromatic elliptically polarized laser field on the tunnel ionization rate. We introduced an additional term in the imaginary part of the classical action due to the Coulomb interaction.

This correction becomes substantially significant in the sub-barrier region, where the electron comes near the singular Coulomb core, influencing the complete tunneling dynamics. To accurately model these effects, we computed the electron trajectory considering the Coulomb forces and derived analytical expressions for both the initial and drift momenta (Petrović et al. 2023). Our results suggest that, in the whole considered ellipticity range, the Coulomb correction provides a significant, orders-in-magnitude, enhanced the total ionization rate without significantly altering its shape.

Our results indicate that including the Coulomb correction not only modifies the energy distribution of the ionized electrons but also results in a narrower momentum distribution compared to models that omit this correction. These insights have significant implications for a broad spectrum of laser-matter interactions and could guide future research efforts in the field.

Acknowledgment: Authors would like to acknowledge the support received from the Science Fund of the Republic of Serbia, #GRANT 6821, Atoms and (bio)molecules-dynamics and collisional processes on short time scale - ATMOLCOL. Our appreciation also goes to the Serbian Ministry of Education, Science and Technological Development (Agreement No. 451-03-66/2024-03/200122).

References

- Laudau, L., Lifschitz, E., 1977, Quantum Mechanics: non-relativistic theory.
Petrović, V., Marković, H. D., Petrović, I., 2023., Results in Physics, 51, 106718.

Bounds on graviton mass from astrometric data of S-stars

Jovanović, P.,¹  Borka Jovanović, V.²  and Borka, D.² 

¹*Astronomical Observatory, Volgina 7, P.O. Box 74, 11060 Belgrade, Serbia*
²*Department of Theoretical Physics and Condensed Matter Physics (020), Vinča Institute of Nuclear Sciences - National Institute of the Republic of Serbia, University of Belgrade, P.O. Box 522, 11001 Belgrade, Serbia*
E-mail: pjovanovic@aob.rs

Here we use a Yukawa-like correction of the Newtonian gravitational potential, proposed by C. Will (see Ref. Jovanović et al. 2024a) in order to obtain new bounds on graviton mass from the observed orbits of S-stars around Sgr A*. We assumed that the orbital precession of these stars is close to the prediction of General Relativity (see the results of GRAVITY Collaboration in 2020 and 2022) for Schwarzschild precession, but with a possible small discrepancy from it. By comparison of the observed orbits of bright stars (Gillessen et al. 2017) in the Galactic center with their simulated orbits in Yukawa-like gravitational potential, we estimated the constraints on the parameters of this modified theory of gravity. With this approach, we were able to constrain the parameter λ of the potential. Moreover, assuming that λ represents the graviton Compton wavelength, we also found the corresponding upper bound of graviton mass. The obtained results were then compared with our previous estimates (Jovanović et al. 2023, Jovanović et al. 2024b), as well as with the estimates of other authors. Also, obtained results are in a good agreement with the corresponding LIGO results.

References

- Gillessen, S.; Plewa, P.M.; Eisenhauer, F.; Sari, R.E.; Waisberg, I.; Habibi, M.; Pfuhl, O.; George, E.; Dexter, J.; von Fellenberg, S.; et al. An Update on Monitoring Stellar Orbits in the Galactic Center. *Astrophys. J.*, 2017, 837, 30.
- GRAVITY Collaboration; Abuter, R.; Amorim, A.; Bauböck, M.; Berger, J.P.; Bonnet, H.; Brandner, W.; Cardoso, V.; Clénet, Y.; de Zeeuw, P.T.; et al. Detection of the Schwarzschild precession in the orbit of the star S2 near the Galactic centre massive black hole. *Astron. Astrophys.* 2020, 636, L5.
- GRAVITY Collaboration; Abuter, R.; Aymar, N.; Amorim, A.; Ball, J.; Bauböck, M.; Berger, J.P.; Bonnet, H.; Bourdarot, G.; Brandner, W.; et al. Mass

- distribution in the Galactic Center based on interferometric astrometry of multiple stellar orbits. *Astron. Astrophys.*, 2022, 657, L12.
- Jovanović, P.; Borka Jovanović, V.; Borka, D.; Zakharov, A.F. Constraints on Yukawa gravity parameters from observations of bright stars. *J. Cosmol. Astropart. Phys.*, 2023, 3, 056.
- Jovanović, P.; Borka Jovanović, V.; Borka, D.; Zakharov, A. F., Constraints on Graviton Mass from Schwarzschild Precession in the Orbits of S-Stars around the Galactic Center, 2024a, *Symmetry* 16, 397
- Jovanović, P.; Borka Jovanović, V.; Borka, D.; Zakharov, A.F., Improvement of graviton mass constraints using GRAVITY's detection of Schwarzschild precession in the orbit of S2 star around the Galactic Center. *Phys. Rev. D*, 2024b, 109, 064046.

SECTIONS (MINI PROJECTS)

M1 A&M DATA and HPC,

M2 A&M DATA and standards,

M3 Modeling the Atmosphere: data&models,

M4 Big data in Astronomy and Earth Observations,

M5 Spectra: stellar and laboratory plasmas,

M6 Radiative & Collisional Processes: databases.

International Meeting on Data for Atomic and Molecular Processes in Plasmas: Advances in Standards and Modelling

November 12-15, 2024, Palić, Serbia

PROGRAMME

Tuesday 12.11.2024. (1 day)	
16:00-17:30	Registration
17:30-18:00	Conference opening
18.00-19.00	Chairs: Vladimir Srećković and Aleksandra Kolarski Lectures Milan Dimitrijević
19.00-21.00	<i>Welcome cocktail</i>

Wednesday 13.11.2024. (II day)	
Session: A&M DATA and HPC Chair: Ognyan Kounchev	
Lectures	
10:00-11:00	Nicolina Pop
11:00-11:30	Mihailo Savić
11:30-12:00	<i>Coffee break</i>
Lectures	
12:00-13:00	Milosavljević Aleksandar
13:00-13:30	Vesna Borka Jovanović
13:30-15:30	<i>Lunch Break</i>
15:30-16:30	Panel discussion: Atmosphere modeling and data, code comparison Chair: Bratislav Marinković
16:30-17:30	Poster session Chair: Bratislav Obradović
17:30-19:00	<i>Mini-excursion</i>
19:00-20:00	Work on mini-projects

Thursday 14.11.2024. (III day)	
Session: DATA and standards Chair: Milorad Kuraica	
Lectures	
10:00-11:00	Ognyan Kounchev
11:00-11:30	Nikola Starčević
11:30-12:00	<i>Coffee break</i>
Lectures	
12:00-13:00	Felix Iacob
13:00-13:30	Zoran Mijić
13.30-15.30	<i>Lunch Break</i>
15:30-16:30	Chair: Felix Iacob Lectures Saša Dujko
16:30-17:30	Poster session Chair: Zoran Mijić
17:30-19:30	Work on mini-projects
20:00-22:00	<i>Conference dinner</i>

Friday 15.11.2024. (IV day)	
Session: Datasets, databases and codes for modeling: problems Chair: Milan Dimitrijević	
Lectures	
10:00-11:00	Aleksandra Kolarski
11:00-11:30	Organizing Committee Meeting
11:30-12:00	Conference closing
12:00	Departure

AUTHORS' INDEX

- Arnaud, F. 69, 71
Banjanac, R.M. 47
Bednár, P. 59
Biagi, P.F. 52
Borka Jovanović, V. 30, 82, 86
Borka, D. 30, 82, 86
Bošnjaković, D.V. 27, 75
Boudjada, M.Y. 52
Bozek, J. 25
Butka, P. 59
Capozziello, S. 82
Christova, M.D. 67
Delibašić Marković, H.S. 84
Dimitrijević, M.S. 10, 67
Djuissi, E. 23
Dragić, A.L. 47
Dujko, S. 27, 72, 75
Eichelberger, H. 57
Iacob, F. 22, 65
Ivanović, S.Đ. 74
Jevremović, S. 71
Joković, D.R. 47
Jovanović, P. 30, 82, 86
Knežević, D. 47
Kolarski, A. 12, 52, 59, 69, 71
Kopyra, J. 81
Kounchev, O. 26
Kovačević, V.V. 79
Krstić, I.B. 77
Kuraica, M.M. 77, 79
Langović, M. 69, 71
Maletić, D.M. 47
Maljković, J.B. 81
Marić, D. 72
Marinković, B.P. 49, 74, 81
Marjanović, J. 72
Mezei, J.Z. 23
Mijić, Z.R. 49, 67
Milosavljević, A.R. 25
Nico, G. 52
Nicolas, C. 25
Nina, A. 52, 59, 69
Obradović, B.M. 77, 79
Petrović, I.D. 84
Petrović, S. 40
Petrović, V.M. 84
Petrović, Z.Lj. 72
Pop, N. 23, 67
Popović, L.Č. 59
Ranitović, P. 79
Robert, E. 25
Sarnovský, M. 59
Savić, M.R. 47
Schneider, I.F. 23
Simeonov, G. 26
Simonović, I.B. 27, 75
Sretenović, G.B. 79
Srećković, V.A. 52, 59, 65, 67, 69, 70, 71
Starčević, N. 40
Tošić, S. 70
Travar, M. 47
Udovičić, V.I. 47
Uskoković, N.A. 74
Veselinović, N.B. 47, 52
Vujčić, V. 65, 67, 70

CIP - Каталогизacija у публикацији
Народна библиотека Србије, Београд

52-355.3(048)

533.9(048)

539.1(048)

INTERNATIONAL Meeting on Data for Atomic and Molecular Processes in Plasmas: Advances in Standards and Modelling (2024 ; Palić)

Book of abstracts and contributed papers / International Meeting on Data for Atomic and Molecular Processes in Plasmas: Advances in Standards and Modelling, November 12-15, 2024, Palić, Serbia ; [organizer Institute of Physics Belgrade] ; edited by Vladimir A. Srećković ... [et al.]. - Belgrade : Institute of Physics, 2024 (Beograd : Skripta Internacional). - 94 str. : ilustr. ; 24 cm

Tiraž 50. - Bibliografija uz većinu apstrakata. - Registar.

ISBN 978-86-82441-69-4

1. Srećković, Vladimir A., 1972- [уредник]

а) Астрофизика -- Апстракти б) Плазма -- Апстракти в) Атомска физика -- Апстракти

COBISS.SR-ID 156258313